Terminal uridylyltransferases target RNA viruses as part of the innate immune system

Terminal uridylyltransferases target RNA viruses as part of the innate immune system

Jérémie Le Pen[1,2,3,†], Hongbing Jiang[4,#], Tomás Di Domenico[1,3,5,#], Emma Kneuss[1,6], Joanna Kosałka[1,3], Christian Leung[4], Marcos Morgan[7,8], Christian Much[7,8], Konrad L. M. Rudolph[1,3,5], Anton J. Enright[9], Dónal O'Carroll[7,8], David Wang[4], Eric A. Miska[* 1,3,5]

[1] Gurdon Institute, University of Cambridge, Tennis Court Road, Cambridge, CB2 1QN, United Kingdom
[2] Department of Biochemistry, University of Cambridge, 80 Tennis Court Road, Cambridge, CB2 1GA, United Kingdom
[3] Department of Genetics, University of Cambridge, Downing Street, Cambridge, CB2 3EH, United Kingdom
[4] Departments of Molecular Microbiology and Pathology & Immunology, Washington University in St. Louis School of Medicine, St. Louis, Missouri, United States of America
[5] Wellcome Trust Sanger Institute, Wellcome Trust Genome Campus, Cambridge, CB10 1SA, United Kingdom
[6] Cancer Research UK, Cambridge Institute, University of Cambridge, Cambridge, CB2 0RE, United Kingdom
[7] MRC Centre for Regenerative Medicine, Institute for Stem Cell Research, School of Biological Sciences, University of Edinburgh, 5 Little France Drive, Edinburgh, EH16 4UU, United Kingdom
[8] European Molecular Biology Laboratory (EMBL), Mouse Biology Unit, Via Ramarini 32, Monterotondo Scalo, 00015, Italy
[9] European Molecular Biology Laboratory (EMBL), European Bioinformatics Institute (EBI), Hinxton, Cambridge, CB10 1SD, United Kingdom
[†] Current address: Laboratory of Virology and Infectious Disease, The Rockefeller University, New York, New York, United States of America

[#] These authors contributed equally

*Correspondence to: Eric A. Miska, email eam29@cam.ac.uk phone +44-1223-767220

RNA viruses are a major threat to animals and plants. RNA interference (RNAi) and the interferon response provide innate antiviral defense against RNA viruses. Here we performed a large-scale screen using *C. elegans* and its natural pathogen, the Orsay virus (OrV), and identified *cde-1* as important for antiviral defense. CDE-1 is a homologue of the mammalian TUT4 and TUT7 (collectively called TUT4(7)) terminal uridylyltransferases; its catalytic activity is required for its antiviral function. CDE-1 uridylates the 3′ end of the OrV RNA genome and promotes its degradation, independently of the RNAi pathway. Likewise, TUT4(7) uridylate influenza A virus (IAV) mRNAs in mammalian cells. Deletion of TUT4(7) leads to increased IAV mRNA and protein levels. We have defined 3′ terminal uridylation of viral RNAs as a conserved antiviral defense mechanism.

RNA viruses are a major threat to human health and food security. Understanding the fundamental mechanisms by which animals and plants combat viral infections might lead to new therapeutic antiviral approaches. RNA interference (RNAi) is an important antiviral pathway in most animals and plants: Dicer recognizes and cleaves the double-stranded viral RNA genome into virus-derived small interfering RNAs (viral siRNAs, viRNAs), which are loaded into Argonaute proteins to form the RNA-induced silencing complex (RISC) that in turn targets the viral RNA genome [1]. Vertebrates have additionally evolved a cellular signaling-based pathway, the interferon response (IR): upon recognition of foreign RNAs (i.e. double-stranded or bearing a 5′ di/triphosphate), cytosolic receptors of the RIG-I family activate the IR which results in an antiviral state of the cell [2,3]. In the evolutionary arms race between viruses and their hosts,

however, animals must have evolved a diverse range of antiviral strategies, to not solely rely on the RNAi or IR pathways.

Here, we develop a system for antiviral gene discovery using the nematode *Caenorhabditis elegans* (*C. elegans*) and identify 3′ terminal uridylation of viral RNAs as a third antiviral mechanism in animals.

RESULTS

A forward genetic screen identifies new genes required for antiviral defense in *C. elegans*

We carried out a forward genetic screen to discover antiviral pathways in animals using *C. elegans* and its natural intestinal pathogen, the Orsay virus (OrV) [4-12]. OrV is a bipartite positive-strand RNA virus related to the *Nodaviridae* [4]. As is typical for positive sense RNA viruses, the genomic strand of the OrV is a template for translation. The OrV spreads horizontally in populations of *C. elegans*: it is taken up orally, infects only intestinal cells and probably exits through defecation [4]. While *C. elegans* lacks an interferon pathway, a RIG-I ortholog, DRH-1, acts in viral recognition. DRH-1 forms a Viral Recognition Complex (ViRC) with the *C. elegans* Dicer (DCR-1) and the RNA-binding protein RDE-4 to link viral recognition to a dedicated antiviral RNAi pathway, involving the Argonaute protein RDE-1 [5,11,13,14]. DRH-1 also induces a transcriptional immune response through a STAT-dependent signaling pathway (e.g. the gene *sdz-6*, as shown by qRT-PCR in Extended Data Fig. 1a) [10,15,16]. However, the antiviral function of the DRH-1-mediated stress response remains to be elucidated. *C. elegans* also elicits a “biotic stress response” upon OrV infection that is independent of DRH-1 and partially overlaps with transcriptional responses induced by other types of pathogens, possibly as

77 a result of perturbations in cell homeostasis and/or mechanical integrity (e.g. the gene *lys-3*,
78 encoding an antibacterial enzyme, as shown by qRT-PCR in Extended Data Fig. 1a) [10]. We
79 generated a viral stress sensor transgene by placing the green fluorescent protein (GFP) under the
80 control of the *lys-3* promoter (allele *mjIs228*; Fig. 1a). Upon infection, the level of GFP
81 expression in the intestine mirrored the viral load in wild type, *drh-1* and *rde-1* mutants
82 (Extended Data Fig. 1b, c). We used chemical mutagenesis to screen ~50,000 haploid genomes
83 (Fig. 1b) and identified 16 isolates we named Ovid (Orsay Virus Immune Deficient; Fig. 1c and
84 Supplementary Table 1). 13 out of 16 *ovid* mutants showed increased viral loads (Fig. 1c). *ovid-*
85 *3,4,5,10,12* are compromised in somatic RNAi, as tested by RNAi knockdown of the gene *unc-*
86 *22*, which normally results in impaired locomation (Fig. 1c), and *ovid-3,4,10* carry new alleles of
87 RNAi genes *mut-16*, *rde-4* and *rrf-1*, respectively (Table 1). To further stratify our Ovid isolates,
88 we assayed DRH-1 pathway activation using the expression of the downstream induced gene
89 *sdz-6* as readout (Fig. 1d). Only *ovid-1* phenocopied *drh-1* mutants and we subsequently
90 demonstrated that *ovid-1* defines a new allele of *drh-1* (Fig. 1d). We identified a number of
91 additional candidate genes (Table 1). *ovid-9* and *ovid-11* mutants are neither defective in
92 canonical RNAi nor in the DRH-1 pathway and thus represent candidate genes for novel antiviral
93 defense mechanisms.
94
95 **The terminal uridylyltransferase CDE-1 is required for antiviral defense in *C. elegans***
96 Whole-genome re-sequencing and genetic complementation tests revealed the causative mutation
97 in *ovid-9* to be a single-nucleotide nonsense mutation in the *cde-1* gene (*mj414*, glutamine 910 to
98 STOP) (Fig. 2a and Extended Data Fig. 2). *cde-1* encodes a catalytically active 3′-terminal RNA
99 uridylyltransferase (TUT), which is a homologue of mammalian TUT4 and TUT7 enzymes [17-19]

(Fig. 2b, c). The independently derived *cde-1* (*tm1021*) knockout strain also phenocopied viral stress sensor activation (Extended Data Fig. 3), high viral loads (Fig. 2d), and horizontal transmission of infection (Extended Data Fig. 3). RNA FISH revealed that viral infection is restricted to the intestine in *cde-1* and in *cde-1; drh-1* double mutants [4,9] (Extended Data Fig. 4a). We validated that CDE-1 is present in the intestine using a GFP fusion [18] (Extended Data Fig. 4b). To disentangle between the functions of CDE-1 in different tissues, *cde-1* was exclusively expressed from an intestine-specific *vha-6p* promoter (Extended Data Fig. 4c). Animals with intestinal expression of *cde-1* became resistant to viral infection (Extended Data Fig. 4d), but kept a defect in meiotic chromosome segregation (Extended Data Fig. 4e), probably caused by CDE-1 depletion in the germline [17]. CDE-1 contains a conserved triad of acid aspartic residues (DDD) in its nucleotidyltransferase domain. Mutation of the corresponding DDD triad to DAD (D1011A) in human TUT4 resulted in loss of catalytic activity [20]. A *cde-1* DAD mutant strain (Fig. 2a,c) showed similar viral susceptibility as the *cde-1* null mutants (Fig. 2d). In summary, we identify CDE-1-mediated 3′ terminal uridylation as an antiviral activity in the intestine of *C. elegans*.

CDE-1 exert its antiviral function independently of antiviral RNAi

In eukaryotes, addition of 3′ uridyl-tails (U-tails) by TUTs is a degradation signal that can engage: (i) the XRN-family of exoribonucleases for 5′ to 3′ RNA decay; (ii) the 3′ to 5′ exoribonuclease DIS3L2; (iii) the 3′ to 5′ exosome complex [21-24]. We sought to identify the RNA(s) targeted by CDE-1 in its antiviral role. CDE-1 is implicated in endogenous RNAi pathways that are restricted to the germline [17]. Small RNA sequencing on whole animals revealed that siRNAs are targeted by CDE-1 for 3′ uridylation, miRNAs are occasionally

targeted, and piRNAs are not targeted [17] (Extended Data Fig. 5a). The role of CDE-1 in small RNA function remains unclear as depletion of CDE-1 leads to only subtle changes in siRNA and miRNA steady state levels (Extended Data Fig. 5b, c). To understand if CDE-1 functions through modification of siRNAs in antiviral immunity, we tested *cde-1* mutants directly for defects in antiviral RNAi. During an antiviral RNAi response in *C. elegans*, the ViRC complex recognizes the dsRNA of the replicating viral genome and dices it into sense and antisense ~23-nt long primary viRNAs, which are loaded into the RDE-1 Argonaute protein [5] (Fig. 3a). The RNAi response is further amplified by RNA-dependent RNA polymerase (RdRP, RRF-1) generated 22-nt long antisense secondary viRNAs, with a 5′ triphosphate guanine (22G-RNAs), which are incorporated into secondary Argonaute proteins to silence viral amplification [5] (Fig. 3a). Thus, in an animal with functional antiviral RNAi, a high viral load should correlate with a high level of viRNAs. We measured primary and secondary viRNAs in different genetic backgrounds (Fig. 3b,c). All the mutants tested (*drh-1*, *rde-1*, *cde-1*) accumulate high levels of the virus as compared to wild type. In *drh-1* mutants, primary and secondary viRNAs are depleted when compared to wild type, despite the increase in viral load. In *rde-1* mutants, primary viRNAs are abundant but secondary viRNAs are depleted, as in *drh-1*. In contrast, *cde-1* mutants accumulate both primary and secondary viRNAs to a level that correlates with the high viral load. To determine if viRNAs can silence viral amplification in *cde-1* mutants, we carried out epistasis analysis using null mutants of *drh-1*, *rde-1* and *cde-1* (Fig. 3d,e). Both *cde-1;drh-1* and *cde-1;rde-1* double mutants showed an increase in viral load as compared to *drh-1* or *rde-1* on its own. We conclude that CDE-1 does not exert its immune function through the antiviral RNAi pathway.

CDE-1 defines a novel antiviral immunity pathway

In mammals, uridylation is coupled to poly(A) tail length where TUT4 and TUT7 (collectively called TUT4(7)) preferentially uridylate mRNAs with short poly(A) tails (<25 nt) to facilitate their degradation [25,26] (Fig. 4a). We thus assessed the impact of CDE-1 on endogenous mRNA poly(A) tail lengths and terminal nucleotide addition in infected wild-type or *cde-1* mutant animals using TAIL-seq [25,27]. The *C. elegans* transcriptome revealed a bimodal distribution of poly(A) tail lengths, with a major peak of poly(A) tails of ~40 nt, and a second peak of poly(A) tails of ~10 nt (Fig. 4b; using our method we could not assess transcripts with poly(A) tails > 79 nt). In *cde-1* mutants, there is a shift of the major ~40 nt peak to ~36 nt and an increase in transcripts with shorter poly(A) (Fig. 4b). We infer that CDE-1 promotes the degradation of transcripts with short poly(A) tails in *C. elegans* too. However, CDE-1 had no global effect on the poly(A) tail distribution of OrV-induced stress response genes (Extended Data Fig. 6a). Also, the OrV-induced stress response was stronger in *cde-1* mutants than in wild-type upon infection (Extended Data Fig. 6b), reflecting the difference in viral load between these two strains. This indicates that CDE-1 is not required for the OrV-induced stress response. Although we cannot formally rule out that CDE-1 may regulate an endogenous target(s), the evidence indicates this is not CDE-1's principal function in antiviral immunity.

Instead, we postulated that the viral RNA genome itself may be uridylated by CDE-1. U-tails can only be observed on a small percentage of cellular RNAs as uridylated RNAs are prone to be degraded [26]. To detect uridylated Orsay RNA degradation intermediates, we carried out 3′ rapid amplification of cDNA ends (RACE) followed by high-throughput sequencing of the OrV RNAs extracted from *C. elegans* two days postinfection (RACE-seq; Extended Data Fig. 7a). Mono(U)

tails constituted the most abundant fraction of non-templated nucleotides detected at the 3′ end of both OrV RNA1 and OrV RNA2 (Fig. 4c-e). For both RNA1 and 2, U-tailing was lost in two independent *cde-1* mutant alleles. In contrast, *drh-1* and *rde-1* mutants showed similar levels of viral RNA U-tails to wild-type, indicating that U-tailing is independent of viral load and that CDE-1 is not in limited quantities (Extended Data Fig. 7b,c). OrV RNA1 and RNA2 have a terminal uridylyl residue in their genome such that the addition of an extra non-templated uridine by CDE-1 forms a UU termination (Fig. 4d), which is a signal for uridylation-dependent RNA decay [21,23]. The two XRN paralogs in *C. elegans* (XRN-1 and XRN-2) and the exosome components (e.g. DIS-3, EXOS-2) are essential [28,29], and these RNA degradation pathways normally act redundantly on uridylated RNAs [26]. We therefore subjected *C. elegans* to a short (24 hours) RNAi treatment to effect a partial knockdown of *cde-1*, the exonuclease *disl-2* (the *C. elegans* DIS3L2 homologue), the exosome components *exos-2* and *dis-3*, and the exonuclease *xrn-2*. Treated animals, which appeared superficially wild type, were infected with OrV for 24 hours. The frequency of U-tails in OrV RNA2 was measured by RACE-seq (Fig. 4f). ~4% of OrV RNA2 were uridylated in animals exposed to the empty vector control RNAi, compared to ~1% in *cde-1* knockdown. RNAi treatments against *disl-2* did not affect the U-tail frequency. We measured a 1.4 to 1.7 fold increase in U-tail frequency upon RNAi treatment against *exos-2*, *dis-3* and *xrn-2*, suggesting that these factors each contribute to the degradation of uridylated viral RNAs, in accordance with a study that shows that DIS3 and the exosome can degrade viral RNAs in *Drosophila* and human cells [30]. We conclude that *C. elegans* uses uridylation of the OrV as an innate immune defense. This mechanism acts in parallel to antiviral RNAi to combat viral infection (Fig. 5).

Terminal uridylyltransferases target viral RNAs in mammalian cells

The U-tail modification is conserved in eukaryotes and could impact a broad range of viruses in a variety of hosts [31]. We tested if U-tailing affects the replication of Influenza A virus (IAV), which can infect human and murine cells. The IAV genome consists of eight antisense RNA segments (viral RNAs, vRNAs) from which the viral RdRP produces: (i) the sense complementary RNAs (cRNAs), which serve as templates to produce more vRNAs; and (ii) the mRNAs that are 3′ polyadenylated and exported to the cytosol for translation into viral proteins [32] (Fig. 6a). We examined the 3′ end of a set of IAV RNAs, at 8 hours post-infection (hpi), in A549 human lung cells by RACE-seq. We could not detect U-tails at the ends of vRNAs or cRNAs. In contrast, viral mRNAs were highly uridylated at their 3′ end, with ~77% of the IAV Nucleoprotein (NP) mRNA containing a U-tail, and a di(U)-tail being the most common type of 3′ end (~32%) (Fig. 6b-e). The IAV NP mRNA is also uridylated (~40-50%) at 8 hpi in mouse embryonic fibroblasts (MEFs), but uridylation was lost in MEFs deficient in both *Tut4* and *Tut7* [25] (Fig. 6f). Thus TUT4(7) can uridylate the 3′ end of viral RNAs in mammalian cells. The RACE-seq can only detect IAV mRNAs with poly(A) tails of <70 nt; it is possible that some IAV mRNAs with very long poly(A) tails are less prone to be uridylated. To test the impact of TUT4(7) on IAV, we measured the quantity of NP mRNA by qRT-PCR in infected MEFs (Extended Data Fig. 8a). The IAV NP mRNA accumulated more rapidly and to a higher level at the peak in MEFs *Tut4(7)* KO cells (peak at 8 hpi) compared to WT cells (peak at 16 hpi) before decreasing later in infection (24 hpi). Consistent with the difference in mRNA levels, the NP mRNA-encoded viral nucleoprotein (NP) accumulated more rapidly in MEFs *Tut4(7)* KO cells compared to WT during the first eight hours of infection (Extended Data Fig. 8b). Accordingly, more infected cells overall were observed in MEFs *Tut4(7)* KO compared to WT (Fig. 6g). In

conclusion, TUT4(7) could act as an early barrier against IAV infection in mammalian cells. Although we cannot rule out that TUT4(7) may impact other steps of the IAV viral cycle, such as entry, our data strongly supports a model where TUT4(7) act by reducing the expression levels of IAV mRNAs during the early stages of IAV infection in MEFs, leading to a decrease in viral protein levels and rates of infection. Future studies will need to address the antiviral function of TUT4(7) in a variety of relevant host-virus models.

DISCUSSION

Previously, we have shown that the antiviral RNAi pathway and DRH-1 are central to the innate immune response of *C. elegans* [5]. Here, we demonstrate that the terminal uridylyltransferases also play a critical role in antiviral immunity, uridylating viral RNAs (with 1-2 Us) to mark them for degradation. It is unclear how terminal uridylyltransferase recognize viral RNAs as *bona fide* targets. Receptors of the RIG-I family commonly recognize pathogen-associated patterns at the 5′ termini of viral RNAs. In contrast, terminal uridylyltransferases interact with the 3′ termini of cytosolic RNAs with no poly(A)-tail or a short poly(A)-tail. As many RNA viruses, like OrV, lack a poly(A) tail at the 3′ termini of their RNA genomes, this may be a pathogen-associated pattern-recognition feature. We speculate that the IAV mRNAs and a fraction of the OrV RNAs are vulnerable to TUTs when exposed in the cytosol for translation. In conclusion, we find that terminal uridylyltransferases are potent antiviral factors during the early stages of RNA virus infections in *C. elegans* and in mammalian cells. This finding supports a scenario where eukaryotic mRNA decay pathways originally evolved as intrinsic cellular defenses against pathogens [33,34]. Vertebrates also benefit from the interferon response and adaptive immune system, serving as potent lines of defense against pathogenic viruses; future studies will thus

need to address the relative importance of antiviral uridylation in whole organisms. Terminal uridylyltransferases are widely conserved in eukaryotes and could potentially target a wide range of RNA viruses [31]. Perhaps as a response to this threat, some viruses evolved to protect their RNA termini, such as single-stranded RNA viruses of the *Flaviviridae* family, which have highly structured 3′ ends resistant to degradation by cellular exonucleases [35]. Our study illustrates that the 3′ termini of viral RNAs are key in the evolutionary arms race between viruses and their hosts.

REFERENCES

1. Ding, S.-W. & Voinnet, O. Antiviral immunity directed by small RNAs. *Cell* **130,** 413–426 (2007).
2. Goubau, D., Deddouche, S. & Reis e Sousa, C. Cytosolic Sensing of Viruses. *Immunity* **38,** 855–869 (2013).
3. Schoggins, J. W. *et al.* A diverse range of gene products are effectors of the type I interferon antiviral response. *Nature* **472,** 481–485 (2011).
4. Félix, M.-A. *et al.* Natural and experimental infection of Caenorhabditis nematodes by novel viruses related to nodaviruses. *PLoS Biol.* **9,** e1000586 (2011).
5. Ashe, A. *et al.* A deletion polymorphism in the Caenorhabditis elegans RIG-I homolog disables viral RNA dicing and antiviral immunity. *Elife* **2,** e00994 (2013).

6. Ashe, A., Sarkies, P., Le Pen, J., Tanguy, M. & Miska, E. A. Antiviral RNAi against Orsay virus is neither systemic nor transgenerational in Caenorhabditis elegans. *J. Virol.* **89,** JVI.03664–14–12046 (2015).

7. Guo, Y. R. *et al.* Crystal structure of a nematode-infecting virus. *Proc. Natl. Acad. Sci. U.S.A.* **111,** 12781–12786 (2014).

8. Jiang, H. *et al.* Orsay virus utilizes ribosomal frameshifting to express a novel protein that is incorporated into virions. *Virology* **450-451,** 213–221 (2014).

9. Franz, C. J. *et al.* Orsay, Santeuil and Le Blanc viruses primarily infect intestinal cells in Caenorhabditis nematodes. *Virology* **448,** 255–264 (2014).

10. Sarkies, P., Ashe, A., Le Pen, J., McKie, M. A. & Miska, E. A. Competition between virus-derived and endogenous small RNAs regulates gene expression in Caenorhabditis elegans. *Genome Res.* **23,** 1258–1270 (2013).

11. Guo, X., Zhang, R., Wang, J., Ding, S.-W. & Lu, R. Homologous RIG-I-like helicase proteins direct RNAi-mediated antiviral immunity in C. elegans by distinct mechanisms. *Proc. Natl. Acad. Sci. U.S.A.* **110,** 16085–16090 (2013).

12. Fan, Y. *et al.* Structure of a pentameric virion-associated fiber with a potential role in Orsay virus entry to host cells. *PLoS Pathog.* **13,** e1006231 (2017).

13. Duchaine, T. F. *et al.* Functional proteomics reveals the biochemical niche of C. elegans DCR-1 in multiple small-RNA-mediated pathways. *Cell* **124,** 343–354 (2006).

14. Tabara, H., Yigit, E., Siomi, H. & Mello, C. C. The dsRNA binding protein RDE-4 interacts with RDE-1, DCR-1, and a DExH-box helicase to direct RNAi in C. elegans. *Cell* **109,** 861–871 (2002).

15. Jiang, H., Chen, K., Sandoval, L. E., Leung, C. & Wang, D. An Evolutionarily Conserved Pathway Essential for Orsay Virus Infection ofCaenorhabditis elegans. *MBio* **8,** e00940–17 (2017).

16. Tanguy, M. *et al.* An Alternative STAT Signaling Pathway Acts in Viral Immunity inCaenorhabditis elegans. *MBio* **8,** e00924–17 (2017).

17. van Wolfswinkel, J. C. *et al.* CDE-1 affects chromosome segregation through uridylation of CSR-1-bound siRNAs. *Cell* **139,** 135–148 (2009).

18. Olsen, A., Vantipalli, M. C. & Lithgow, G. J. Checkpoint proteins control survival of the postmitotic cells in Caenorhabditis elegans. *Science* **312,** 1381–1385 (2006).

19. Kwak, J. E. & Wickens, M. A family of poly(U) polymerases. *RNA* **13,** 860–867 (2007).

20. Heo, I. *et al.* TUT4 in concert with Lin28 suppresses microRNA biogenesis through pre-microRNA uridylation. *Cell* **138,** 696–708 (2009).

21. Norbury, C. J. Cytoplasmic RNA: a case of the tail wagging the dog. *Nat. Rev. Mol. Cell Biol.* **14,** 643–653 (2013).

22. Wickens, M. & Kwak, J. E. Molecular biology. A tail tale for U. *Science* **319,** 1344–1345 (2008).

23. Lee, M., Kim, B. & Kim, V. N. Emerging roles of RNA modification: m(6)A and U-tail. *Cell* **158,** 980–987 (2014).

24. Rissland, O. S. & Norbury, C. J. Decapping is preceded by 3' uridylation in a novel pathway of bulk mRNA turnover. *Nat. Struct. Mol. Biol.* **16,** 616–623 (2009).

25. Morgan, M. *et al.* mRNA 3′ uridylation and poly(A) tail length sculpt the mammalian maternal transcriptome. *Nature* **548,** 347–351 (2017).

26. Lim, J. *et al.* Uridylation by TUT4 and TUT7 marks mRNA for degradation. *Cell* **159,** 1365–1376 (2014).

27. Chang, H., Lim, J., Ha, M. & Kim, V. N. TAIL-seq: Genome-wide Determination of Poly(A) Tail Length and 3′ End Modifications. *Mol. Cell* **53,** 1044–1052 (2014).

28. Miki, T. S., Rüegger, S., Gaidatzis, D., Stadler, M. B. & Großhans, H. Engineering of a conditional allele reveals multiple roles of XRN2 in Caenorhabditis elegans development and substrate specificity in microRNA turnover. *Nucleic Acids Res.* **42,** 4056–4067 (2014).

29. Kamath, R. S. *et al.* Systematic functional analysis of the Caenorhabditis elegans genome using RNAi. *Nature* **421,** 231–237 (2003).

30. Molleston, J. M. *et al.* A conserved virus-induced cytoplasmic TRAMP-like complex recruits the exosome to target viral RNA for degradation. *Genes Dev.* **30,** 1658–1670 (2016).

31. Huo, Y. *et al.* Widespread 3'-end uridylation in eukaryotic RNA viruses. *Sci Rep* **6,** 25454 (2016).

32. Samji, T. Influenza A: understanding the viral life cycle. *Yale J Biol Med* **82,** 153–159 (2009).

33. Rehwinkel, J. Is anti-viral defence the evolutionary origin of mRNA turnover? (Comment on DOI 10.1002/bies.201600100). *Bioessays* **38,** 817–817 (2016).

34. Hamid, F. M. & Makeyev, E. V. Exaptive origins of regulated mRNA decay in eukaryotes. *Bioessays* **38,** 830–838 (2016).

35. Manokaran, G. *et al.* Dengue subgenomic RNA binds TRIM25 to inhibit interferon expression for epidemiological fitness. *Science* **350,** 217–221 (2015).

METHODS

Genetics

Animals were grown on agar plates, at 20°C, and fed with *E. coli* strain HB101 (obtained from the *Caenorhabditis* Genetics Center, University of Minnesota, USA). Standard *C. elegans* procedures were used for maintenance and genetic crosses [36]. The wild-type strain refers to Bristol N2 unless stated otherwise. All strains used in this study are listed in the Supplementary Table 2.

PCR primers

All PCR primers used in this study are listed in the Supplementary Table 3.

Viral filtrate preparation

Viral filtrate was prepared as in [8]. Briefly, JU1580 animals were first stably infected by the Orsay virus (OrV) in solid culture and then transferred in a liquid culture containing OP50 bacteria for seven days. The liquid culture with infected JU1580 was then centrifuged at 16,000 g for 30 min and the supernatant was filtered (0.22 µm filter) to produce the viral filtrate (stored at -80°C).

Transgenesis of *C. elegans* with the *lys-3p::GFP* viral stress sensor

The 452 bp region upstream of the *lys-3* start codon and the first 57 bp of the coding region of *lys-3* were used as a promoter and cloned into an entry clone using Multi-Site Gateway cloning (Invitrogen) according to manufacturer's instructions. The *lys-3* donor plasmid was validated by

sequencing. Gateway technology was then used to clone the *lys-3* fragment in frame with a GFP cDNA. The 3′ UTR of the *tbb-2* (tubulin, beta) gene was used. The *lys-3p::GFP:tbb-2-3'UTR* plasmid was amplified and purified according to Invitrogen's instruction. The *C. elegans* microinjection mix was: 5 ng/µl plasmid *lys-3p::GFP:tbb-2-3'UTR*; 5 ng/µl co-injection marker (*myo-2::mcherry::unc-54-3'UTR*, pharynx expression) and 85 ng/µl 1 kb Invitrogen ladder in 1× injection buffer (20 mM potassium phosphate, 3 mM potassium citrate, pH 7.5). This mix was microinjected into the gonads of *rde-1* (*ne219*) mutants to generate a multicopy extrachromosomal array (allele *mjEx547*). X-ray integration of the transgene into the *C. elegans* genome was performed as described previously [37]. Animals carrying an integrated transgene (allele *mjIs228*) were outcrossed three times to generate SX2635 (lacking *ne219*), referred to as wild-type viral stress sensor strain in this study.

Confocal images of the biostress reporter

A 2% agar pad was used on top of a glass slide and a drop of 10 µM tetramisol in M9 medium was placed on this agar pad. Animals were picked into the tetramisol solution. Imaging was performed with an Olympus Upright FV1000 microscope at 10× or 20× magnification, as specified, using the FluoView image software (Olympus). Identical microscope settings were used for all images within a figure.

Forward genetic screen for Ovid screen isolates

Approximately 4,000 viral stress sensor transgenic animals were mutagenized using ethyl methanesulfonate (EMS) as described in [36] and [38]. Approximately 50,000 F2 animals were infected for 3-4 days and ~2,000 animals showing intestinal GFP were picked individually for

re-testing. 16 F2 families showed transmission of the viral stress sensor activation. Bleach treatment confirmed that removing OrV lead to a loss of intestinal GFP signal.

C. elegans infection by the Orsay virus

Animals were either infected for four days as asynchronous populations or for two days as synchronous populations. Infections of asynchronous populations were performed as in [5]. Briefly, two L4 hermaphrodites were distributed in each 50 mm plates and, on the next day, 20 µl of viral filtrate was spread on the plates. Animals were harvested (for viral load measurement) or observed under a Leica M165 FC fluorescent microscope (for scoring of the viral stress sensor) four days post-infection (4 dpi). This method was typically used for the characterization of the Ovid screen isolates. For the infection of synchronous populations, 200 animals at the larval stage L1 were deposited on each 50 mm plate. On the next day, L2 animals were infected with 20 µl of viral filtrate homogeneously spread on the plate. Plates were kept up-side-up for 24 hrs. Animals were harvested for viral load measurement at 2 dpi. This method was used to measure the viral load in *cde-1* mutants, as indicated in the figure legends.

RNA level measurement by qRT-PCR

Harvested animals were washed three times by pelleting-resuspension in M9 solution. Lysis and qRT-PCR was then performed from 5 µl of animal pellet using the Power SYBR Green Cells-to-Ct kit (Ambion, Austin, TX) as described in [5]. The primers M1835 and M1836 [13], and M4410 and M4411 [4], were used to measure RNA levels of *gapdh* and OrV gRNA1, respectively.

RNAi-mediated knockdown of *unc-22*

All the bacterial feeding clones used in this study were a kind gift from the laboratory of Julie Ahringer. Bacteria were grown in LB-Ampicillin (50 μg/ml) for 6 hrs, then seeded onto 50 mm NGM agar plates containing 1 mM IPTG and 25 μg/ml Carbenicillin at a volume of 300 μl bacterial culture per plate and left to dry at room temperature, protected from the light, for 48 hrs. Two L4 animals were picked onto each RNAi plates and the young adult progeny were scored for the phenotype of interest after five days.

Transgenesis of *C. elegans* with the CDE-1::GFP fosmid and imaging

The modified fosmid WRM064A_D06 where the GFP sequence is added at the N-terminal end of *cde-1* was provided by the TransgeneOme Project (Max Planck Institute of Molecular Cell Biology and Genetics, TransgeneOme Unit, Pfotenhauerstr. 108, 01307 Dresden, Germany; construct 09318202437763223 H08) [39]. The construct was injected into the gonad of N2 animals to produce an extrachromosomal array (as described for the biostress reporter), using a *myo-3p::mCherry::unc-54-3'UTR* construct as a co-injection reporter. Transgenic animals (strain SX3123; allele *mjEx594*) were imaged with an Olympus Upright FV1000 microscope at 10x magnification.

Fluorescence in situ hybridization of the Orsay virus RNA2

Animals were harvested in 15 ml of nanopure water and washed three times by pelleting-resuspension in nanopure water. Animals were then transferred to 1.5 ml tubes with a glass pipette. 1 ml of fixative solution (4% formaldehyde in 1X PBS) was added and samples were incubating at room temperature, on a rotating wheel, for 45 min. Nematodes were then washed twice by pelleting-resuspension in 1 ml of 1x PBS. Pellet of animals was resuspended in 1 ml

70% ethanol and stored at 4°C. After removal of the ethanol, fixed nematodes were washed once in 1 ml of wash solution (10% formamide, 2X SSC). The animal pellet was resuspended in 100 µl of hybridization solution (10% dextran sulfate, 2X SSC, 10% formamide) with 1 µl 1:50 of the probe v1580-RNA2-TexRed (ACCATGCGAGCATTCTGAACGTCA), a kind gift of Marie-Anne Félix, and incubated overnight at 30°C protected from the light. The next day, animals were washed three times in wash solution by pelleting-resuspension. Eventually, animals were resuspended in 1 ml wash solution with DAPI and incubated at 30°C for 30 min. Samples were centrifuged and supernatant was discarded. The animal pellet was resuspended in 1 ml of 2X SSC solution and stored at 4°C protected from light. Animals were then placed on a glass slide, in a drop of Vectashield anti-fade solution (Vector). Imaging was performed on an Olympus Upright FV1000 at 40x magnification, using the FluoView image software (Olympus). Same settings of fluorescence were used for all images compared.

Transgenesis of *C. elegans* with the *vha-6p::gfp* plasmid and viral load measurement

The 878 bp region upstream of the *vha-6* start codon was used as a promoter and cloned into an entry clone using Multi-Site Gateway cloning (Invitrogen) according to manufacturer's instructions. The *vha-6p* donor plasmid was validated by sequencing. Gateway technology was then used to clone the *vha-6p* upstream of (i) the GFP cDNA, or (ii) the full length *cde-1* gene (from ATG to STOP with endogenous introns). The 3′ UTR of the *tbb-2* (tubulin, beta) gene was used. The *vha-6p::GFP::tbb-2-3'UTR* and *vha-6p::cde-1::tbb-2-3'UTR* plasmids were amplified and purified according to Invitrogen's instruction. The *C. elegans* microinjection mix was: 10 ng/µl plasmid *vha-6p::GFP:tbb-2-3'UTR*; 10 ng/µl plasmid *vha-6p::cde-1::tbb-2-3'UTR;* 5 ng/µl co-injection marker (*myo-2::mcherry::unc-54-3'UTR*, pharynx expression) and 75 ng/µl 1 kb Invitrogen ladder in 1× injection buffer (20 mM potassium phosphate, 3 mM potassium citrate,

pH 7.5). This mix was microinjected into the gonads of *cde-1* (*tm1021*) mutants to generate a multicopy extrachromosomal array (allele *mjEx595*). *vha-6p* driven GFP expression was only observed in the intestine. 100 animals carrying the extrachromosomal array were manually selected for infection (from the L2 larval stage to young adult).

Small RNA sequencing

Small RNA libraries were prepared from infected animals as previously described in [5]. We used pellets of animals, washed three times in M9 solution and resuspended in 1 ml of TriSure (Bioline) as a starting material. RNA extraction was performed according to manufacturer's instructions. Some populations of siRNAs (including secondary viRNAs) contain a characteristic 5′ triphosphate group that has to be replaced by a 5′ monophosphate to allow the 5′ ligation step of the library preparation. For this purpose, 1 µg of RNA was put in solution with 1X 5′p polyphophatase buffer and 1 µl of 5′ polyphophatase (Epicentre) for a total volume of 20 µl, incubated for 30 min at 37°C and then submitted to phenol purification and resuspended in 5 µl of nuclease-free water. Treated RNA sample was entirely used as starting material for the TruSeq Small RNA kit (Illumina), following the manufacturer's instructions, to make the so-called 5′ independent libraries. So-called 5′ dependent libraries were made by a similar procedure but without polyphophatase treatment, so that only 5′ monophosphate siRNAs (such as primary viRNAs) could be cloned. Libraries were submitted to the Gurdon Institute sequencing facility for Illumina HiSeq sequencing (SR36). Small RNA sequencing data was aligned to the Ensemble WBcel235 release of the *C. elegans* genome using STAR [40] (v2.5.1b). Briefly, the aligner will allow untemplated residues at the ends of an aligned sequence when run in local mode.

462 Untemplated 3′ sequences were extracted and analysed using custom Python scripts. Details of
463 the analyses for each small RNA subtype can be found in the source code. For miRNA
464 differential expression, reads were counted against the miRBase miRNA annotations
465 (miRBase21 hairpins, WBcel235 genome) using featureCounts [41] (v1.5.0-p1). Differential
466 expression analysis was performed on the counts using DESeq2 [42] (v1.10.1).
467
468 **CRISPR/Cas9 for *cde-1* catalytic dead mutant**
469 A CRISPR/Cas9-mediated mutation of *cde-1* was generated as previously described [43]. Guide
470 RNA: UUUGCUGUCAAAUCCUUUGG. Homologous recombination template:
471 TCAGCTATTGCTATTTGTTTGAGATTCGGAGATGGAGATGTTCCGCCTAAAGACTTG
472 ACAGCAAAAGAAGTTATTCAGAAAACTGAATCCGTTCTCAGAAAATGTCATTT. Only
473 the D1069A missense mutation was introduced, as verified by sequencing.
474
475 **TAIL-seq**
476 The TAIL-seq was performed as previously described in [27]. Tail-seq libraries were processed
477 using Tailseeker 2 [27]. The 5′ and 3′ libraries were subsequently adapter trimmed using cutadapt
478 1.10 [44] with Illumina small RNA-seq adapters and filtered to a minimum length of 5bp. Trimmed
479 5′ reads were mapped with STAR 2.5.2a [40] against a combined meta-genome consisting of the
480 *C. elegans* reference genome WBcel235 [45] and the OrV genome [4]. Mapping was performed in
481 end-to-end mode allowing no mismatches and a gap opening and extension penalty of 10,000.
482 Reads were assigned to genes with bedtools 2.26.0 [46]. Subsequently, 3′ reads without poly(A) tail
483 or too many dark cycles were removed from the data. For the subsequent analysis, all *C. elegans*
484 tags with poly(A) tail length equal to zero were discarded. Average poly(A) tail lengths and

uridylation lengths for each sample were calculated as the arithmetic mean weighted by the support for each tag, reported by Tailseeker 2. The complete code is at https://github.com/klmr/poly-u/tree/submitted.

mRNA libraries for deep sequencing

mRNA libraries were prepared from three independent infections, using the NEBNext Ultra RNA non-directional Library kit with poly(A) selection (NEB), according to manufacturer's instructions. Libraries were submitted to the Gurdon Institute sequencing facility for Illumina HiSeq sequencing (SR30). Differentially expressed genes were then called using EdgeR [47].

3′ RACE-seq on the Orsay virus RNAs

The 3′ RACE was performed on the same RNA input than that used for small RNA libraries, without polyphosphatase treatment. 200 ng of RNA were submitted to 3′ ligation using the TruSeq Small RNA kit (Illumina), following the manufacturer's instructions. 3′ ligated RNA was used for reverse-transcription, still using the TruSeq Small RNA kit whilst bypassing the 5′ ligation step. The 3′ end of OrV RNA1 (or RNA2) genome was amplified by PCR ("PCR1") from 2 µl of cDNA, using the primers M7454 and M7456 (or M7455 and M7456) and the Phusion High-Fidelity Taq Polymerase (NEB) with CG buffer, according to manufacturer's instructions. The thermocyler was programmed to 30 seconds at 98°C; 15 cycles of 5 seconds at 98 °C followed by 20 seconds at 60°C and 10 seconds at 72°C. The 5′ adapter sequence from the TruSeq Small RNA kit was then introduced at the 5′ end of the amplicons by PCR ("PCR2") using the primers M7456 and M7601 for OrV RNA1 (or M7456 and M7602 for the OrV RNA2),

using 2 µl of 1/10 diluted amplicon from PCR1 as a template and the same PCR conditions than that used in PCR1. The amplicons from PCR2 were purified using the DNA Clean & Concentrator-5 kit (Zymo Research) and resuspended in 10 µl of water. Resulting DNA was used as an input for the PCR amplification step of the TruSeq Small RNA kit, following the manufacturer's instructions. Libraries were submitted to the Gurdon Institute sequencing facility for Illumina HiSeq sequencing (PE100). The libraries were run on a 10% polyacrylamide gel for size selection (the amplicons could be visualized under UV light and the bands were cut at the same distance of migration for all samples). Paired-end reads obtained from the 3′ RACE experiment on the viral genome show overlap. The PEAR software [48] was used to merge the paired reads into a single read (v0.9.6, default parameters). Merged reads not starting with the targeted 3′ viral genome sequence fragment were discarded. The targeted viral genome sequence was removed from the remaining reads using custom python scripts (https://github.com/tdido/cde-1_analysis). The resulting sequences representing the untemplated tails were analyzed using custom python scripts.

RNAi-mediated knockdown of *exonucleases*

Synchronized animals were grown on normal HB101 food until the L2 larval stage and then transferred RNAi food. Animals were left on RNAi plate (24 hours prior to infection) and infected for 24 hours, from the old L3/young L4 larval stages to adult. RACEseq was performed as described above.

Cell culture

MEF cells were cultured with DMEM (GIBECO) supplemented with 12.5% FBS, 2mM L-glutamine, non-essential amino acid,100 units/ml penicillin/streptomycin, 100 uM β-mercaptoethanol (Sigma). Cells were splitted 1:4 and passaged every three days. A549 cells were cultured with DMEM (GIBECO) supplemented with 10% FBS, 2mM L-glutamine, non-essential amino acid,100 units/ml penicillin/streptomycin and 25mM HEPES.

Cell lines used in this study

All cell lines were tested for negative for mycoplasma. *Tut4(7)* CTR and KO MEFs were derived from E13.5 embryos from crosses of $Tut4^{+/fl};Tut7^{+/fl};R26^{+/+}$ and $Tut4^{+/fl};Tut7^{+/fl};R26^{ERT\text{-}cre/ERT\text{-}cre}$ mice by standard procedures and immortalized at passage 2 by two consecutive infections with pBabeSV40LT. Cre-mediated deletion to obtain *Tut4(7)* null alleles was induced with 600 nM 4-hydroxytamoxifen for three days [25]. All mice used in this study were bred and maintained in EMBL Mouse Biology Unit, Monterotondo, and subsequently in the Centre for Regenerative Medicine, Edinburgh. All procedures were done in accordance to the current Italian legislation (Art. 9, 27. Jan 1992, nu116) under license from the Italian health ministry or the UK Home Office regulations, respectively.

A549 and MEF cells infection by Influenza A virus and RACE-seq

Influenza A virus (A/WSN/1933, H1N1) used in this study was titrated on MDCK cells. All the inoculation MOI of influenza A virus described here and below was calculated as an equivalent MOI on the originally titrated MDCK cells.

A549 or MEF cells were trypsinized and seeded as 2X10^6 cells per T25 flask one day before infection. 16 hours after seeding, culture media were removed and cells were washed once with

pre-warmed DMEM. Influenza A virus (A/WSN/1933, H1N1) were inoculated at MOI 3 diluted with 1000 µl DMEM supplemented with 0.1% BSA (D0.1B). Cells were trypsinized and collected 8 hours post infection. 750 µl TRIzol were added into each infected sample and were then freezed at -80 °C. RNA extraction was performed according to the standard TRIzol procedure.

For the A549 RACE-seq, 2 µg of RNA were submitted to 3′ ligation using the TruSeq Small RNA kit (Illumina), following the manufacturer's instructions. 3′ ligated RNA was used for reverse-transcription, still using the TruSeq Small RNA kit (except that the Invitrogen Suprescript III was used instead of the Superscript II) whilst bypassing the 5′ ligation step. The RT final volume was 12.5 µl. After the RT, water was added to the samples to reach 18.5 µl, final volume. The 3′ end of IAV RNAs were amplified by PCR ("PCR1") from 2 µl of cDNA, using the left primers M8443, M8444, M8451, M8452, M8453, M8454, M8455, M8456 (depending on the target, see the Supplementary Table 3) with the right primer M7456 and the NEB Q5 polymerase, according to manufacturer's instructions (25 µl reaction). The thermocyler was programmed to 30 seconds at 98°C; 5 cycles of 5 seconds at 98 °C followed by 20 seconds at 60°C and 20 seconds at 72°C. Each PCR product was purified using the DNA Clean & Concentrator-5 kit (Zymo Research) and eluted in 11 µl of water. The 5′ adapter sequence from the TruSeq Small RNA kit was then introduced at the 5′ end of the amplicons by PCR ("PCR2") using the left primers M8459, M8460, M8467, M8468, M8469, M8470, M8471, M8472 (depending on the target, see the Supplementary Table 3) with the right primer M7601, using 10 µl of purified PCR1 amplicon as a template and the same PCR conditions that used in PCR1. Again, the amplicons from PCR2 were purified using the Zymo columns and eluted in 11 µl of water. Resulting DNA was used as an input for the PCR amplification step of the TruSeq Small

RNA kit, following the manufacturer's instructions. Libraries were submitted to the Gurdon Institute sequencing facility for Illumina HiSeq sequencing (PE100). The libraries were run on a 10% polyacrylamide gel for size selection (the amplicons could be visualized under UV light and the bands were cut at the same distance of migration for all samples). Paired-end reads obtained from the 3′ RACE experiment on the viral genome show overlap. The PEAR software [48] was used to merge the paired reads into a single read (v0.9.6, default parameters). Merged reads not starting with the targeted 3′ viral RNA sequence fragment were discarded. The targeted viral genome sequence was removed from the remaining reads using custom python scripts (https://github.com/tdido/cde-1_analysis). The resulting sequences representing the untemplated tails were analyzed using custom python scripts. The MEFs RACE-seq was identical to the A549 cells RACE-seq, except: (i) the starting material was 1 µg, (ii) the Invitrogen Superscript II was used for the RT, (iii) PCR1 and PCR2 had 10 cycles each.

MEFs infection by Influenza A virus and qRT-PCR

MEF cells were trypsinized and seeded as 8X10^4 cells per well of 24-well plate one day before infection. 16 hours after seeding, culture media were removed and cells were washed once with pre-warmed DMEM. Influenza A virus (A/WSN/1933, H1N1) were inoculated at MOI 3 diluted with 250 ul DMEM supplemented with 0.1% BSA (D0.1B). Cells were trypsinized and collected 8, 16 and 24 hours post infection. 350 ul TRIzol were added into each infected sample. RNA was extracted using Direct-zol™ RNA MiniPrep (Zymo Research) purification according to the manufacture's protocol and was finally eluted into 60 ul RNase/DNase free water. The extracted RNA was subjected to strand specific qRT-PCR to quantify influenza virus replication as described in [49].

599

600 **MEFs infection by Influenza A virus and FACS assay**

601 MEF cells were trypsinized and seeded as 1X10^4 cells per well of 96-well plate one day before
602 infection. 16 hours after seeding, culture media were removed and cells were washed once with
603 pre-warmed DMEM. Influenza A virus (A/WSN/1933, H1N1) were inoculated at MOI 3 diluted
604 with 50 µl DMEM supplemented with 0.1% BSA (D0.1B). Inoculum was removed after 1 hour
605 of incubation at 37 °C. The infected cells were cultured with MEF cell culture medium with
606 2.5% FBS. 8 hours post inoculation, culture media were removed and cells were trypsinized
607 through incubation with 30 µl 0.05% trypsin for 3 minutes at 37 °C. Trypsinized cells were
608 resuspended with 70ul of P2F (PBS with 2% FBS) and then fixed with 100 µl 4% PFA for 15
609 minutes. Fixed cells were centrifuged at 300g for 5 minutes and then washed once with 100 µl
610 P2F. Cells were then permeablized with buffer (0.1% Saponin, 10mM HEPES, 0.025% Sodium
611 Azide in 1XHBSS) for 15 minutes at room temperature and then spinned at 500g for 2 minutes
612 to remove buffer. Primary anti-influenza A virus nucleoprotein antibodies were purchased from
613 Millipore (MAB8258B | clone A3, biotin-conjugated). The primary antibodies were diluted
614 1:2000 in permeable buffer and 50 µl diluted antibodies were added into each well of 96-well
615 plate. Primary antibodies were incubated with infected cells at room temperature for 1 hour. The
616 cells were then washed 3 times with permeable buffer. FITC conjugated goat anti-mouse
617 secondary antibodies were purchased from Invitrogen and diluted at 1:1000 in permeable buffer.
618 Secondary antibodies were incubated for 1 hour at room temperature and washed as described
619 before. The stained cells were finally resuspended in 70 µl P2F. The cell suspension was run on a
620 high throughput FACS machine (MACSQuant® analyzer 10 - Miltenyi Biotec). Uninfected cells
621 were stained the same as infected cells and were used as negative staining cell populations. Any

622 cells/events that had fluorescence intensity higher than all the negative staining cell population
623 were gated as virus infection positive. Data were analyzed using flowjo software (version 10).
624
625 **Statistics and reproducibility**
626 Statistics as shown in the figure legends. Table 1: *ovid-9* data was reproduced in an independent
627 experiment, data on other Ovid isolates only produced in the shown experiment. *ovid-9* GFP and
628 RNAi scoring not blinded but reproduced by different authors. Fig. 1: *ovid-9* data was
629 reproduced in an independent experiment, data on other Ovid isolates only produced in the
630 shown experiment. Paralyzed animals were not moving even after tapping the plate. Twitching
631 animals were moving but distinctively twitching laterally. Fig. 2: reproduced in an independent
632 experiment (except for the DAD catalityc mutant, only produced in the shown experiment). Fig.
633 3: reproduced in an independent experiment. Fig. 4b: only produced in the shown experiment.
634 Fig. 4d,e: reproduced in an independent experiment. Fig. 4f: only produced in the shown
635 experiment. Fig. 6b,f: only produced in the shown experiment. Figure 6g: reproduced in an
636 independent experiment. Supp. Fig. 1a: only produced in the shown experiment, corroborates
637 published data as cited in the text. Supp. Fig. 1b: at least two pictures taken by condition, except
638 for the male for which the only picture available is shown in the manuscript, all phenotypes
639 (including in males) were observed multiple times. Supp. Fig. 2: reproduced in an independent
640 experiment but with 28 F4 families instead of 64 F8 families. Not blinded but reproduced by
641 different authors. Supp. Fig. 3: only produced in the shown experiment. Not blinded. Supp. Fig.
642 4a: only produced in the shown experiment, at least two pictures per condition. Supp. Fig. 4b:
643 only produced in the shown experiment, at least two pictures per condition, corroborates
644 published data as cited in the text. Supp. Fig. 4d,e: only produced in the shown experiment.

Supp. Fig. 5a-c: only produced in the shown experiment, corroborates published data as cited in the text. Supp. Fig. 6a,b: only produced in the shown experiment. Supp. Fig. 7: reproduced in an independent experiment. Supp. Fig. 8: reproduced in an independent experiment.

Data availability statement

All raw sequencing data are deposited in GEO (small RNA sequencing: GSE80169; mRNA sequencing: GSE76901; TAILseq: GSE85893). All *C. elegans* strains created in this study will be freely available on a non-collaborative basis. Correspondence and requests for materials should be addressed to E.A.M. (eam29@cam.ac.uk).

METHODS-ONLY REFERENCES

36. Brenner, S. The genetics of Caenorhabditis elegans. *Genetics* **77,** 71–94 (1974).
37. Fire, A. Integrative transformation of Caenorhabditis elegans. *EMBO J.* **5,** 2673–2680 (1986).
38. Jorgensen, E. M. & Mango, S. E. The art and design of genetic screens: caenorhabditis elegans. *Nat. Rev. Genet.* **3,** 356–369 (2002).
39. Sarov, M. *et al.* A genome-scale resource for in vivo tag-based protein function exploration in C. elegans. *Cell* **150,** 855–866 (2012).
40. Dobin, A. *et al.* STAR: ultrafast universal RNA-seq aligner. *Bioinformatics* **29,** 15–21 (2013).
41. Liao, Y., Smyth, G. K. & Shi, W. featureCounts: an efficient general purpose program for assigning sequence reads to genomic features. *Bioinformatics* **30,** 923–930 (2014).

42. Love, M. I., Huber, W. & Anders, S. Moderated estimation of fold change and dispersion for RNA-seq data with DESeq2. *Genome Biol.* **15,** 550 (2014).

43. Paix, A., Folkmann, A., Rasoloson, D. & Seydoux, G. High Efficiency, Homology-Directed Genome Editing in Caenorhabditis elegans Using CRISPR-Cas9 Ribonucleoprotein Complexes. *Genetics* **201,** 47–54 (2015).

44. Martin, M. Cutadapt removes adapter sequences from high-throughput sequencing reads. *EMBnet.journal* **17,** 10 (2011).

45. Harris, T. W. *et al.* WormBase 2014: new views of curated biology. *Nucleic Acids Res.* **42,** D789–93 (2014).

46. Quinlan, A. R. & Hall, I. M. BEDTools: a flexible suite of utilities for comparing genomic features. *Bioinformatics* **26,** 841–842 (2010).

47. Robinson, M. D., McCarthy, D. J. & Smyth, G. K. edgeR: a Bioconductor package for differential expression analysis of digital gene expression data. *Bioinformatics* **26,** 139–140 (2010).

48. Zhang, J., Kobert, K., Flouri, T. & Stamatakis, A. PEAR: a fast and accurate Illumina Paired-End reAd mergeR. *Bioinformatics* **30,** 614–620 (2014).

49. Kawakami, E. *et al.* Strand-specific real-time RT-PCR for distinguishing influenza vRNA, cRNA, and mRNA. *J. Virol. Methods* **173,** 1–6 (2011).

ACKNOWLEDGMENTS

We thank Mélanie Tanguy for OrV viral filtrates, Lise Frézal for help with the OrV RNA FISH, Isabel Wilkinson for support with the genetic screen, Nicolas J. Lehrbach for help with microinjections, and Marc Ridyard for lab management. We thank Kay Harnish, Fabian

691 Braukmann and Sylviane Moss for high-throughput sequencing support. We are grateful to V.
692 Narry Kim and Hyeshik Chang for sharing information on TAIL-seq and Adrianus C.M. Boon
693 for providing IAV. We thank Alyson Ashe and Peter Sarkies for their theoretical input on the
694 screen design. We thank the International *C. elegans* gene knockout consortium and the
695 TransgeneOme project for providing reagents. We thank Vladimir Benes and the EMBL genome
696 core for sequencing support. We thank George Allen and Charles Bradshaw for core
697 bioinformatics support. We thank Ragini Medhi and Dick Zijlmans for help with TUTs Western
698 blots. This work was supported by Cancer Research UK (C13474/A18583, C6946/A14492), the
699 Wellcome Trust (104640/Z/14/Z, 092096/Z/10/Z) and The European Research Council (ERC,
700 grant 260688). DW holds an Investigator in the Pathogenesis of Infectious Disease Award from
701 the Burroughs Wellcome Fund.

702

703 AUTHOR INFORMATION

704 The authors have made the following declarations about their contributions: Conceived and
705 designed the experiments: J.L.P., H.J., E.A.M. Performed the experiments: J.L.P., H.J., E.K.,
706 J.K., C.L., M.M., C.M. Analyzed the data: J.L.P., H.J., T.D.D., K.L.M.R., A.J.E, D.O.C., D.W.,
707 EAM. Wrote the manuscript: J.L.P., E.A.M.

708

709 TABLES

710 **Table 1 | Ovid screen candidate genes**

Genotype	High viral load?	RNAi intact?	High sdz-6 level?	Candidate gene	Candidate variation	Brief description
WT	No	Yes	Yes			
rde-1	Yes	No	Yes			RNAi factor

drh-1	Yes	Yes	No			Viral RNA receptor
ovid-1	Yes	Yes	No	*drh-1*	Glu834Lys	Viral RNA receptor
ovid-2	Yes	Yes	Yes	n.d.		
ovid-3	Yes	No	Yes	*mut-16*	Gln861*	RNAi factor
ovid-4	Yes	No	Yes	*rde-4*	Ala220Thr	RNAi factor
ovid-5	Yes	No	Yes	n.d.		
ovid-6	Yes	Yes	Yes	T09B4.2	Pro330Leu	Putative rho guanine nucleotide exchange factor
ovid-7	Yes	Yes	Yes	C41D11.6	Gly596Ser	Putative RNA nuclease
ovid-8	Yes	Yes	Yes	n.d.		
ovid-9	Yes	Yes	Yes	*cde-1*	Gln910*	Terminal uridylyltransferase
ovid-10	Yes	No	Yes	*rrf-1*	Gly45Glu	RNAi factor
ovid-11	Yes	Yes	Yes	C54D10.14	Gly122Arg	Uncharacterized, DRH-1-dependent induction
ovid-12	Yes	No	Yes	F27D4.6	Arg717*	Uncharacterized
ovid-13	n.s.	Yes	Yes	n.d.		
ovid-14	n.s.	Yes	Yes	n.d.		
ovid-15	n.s.	Yes	Yes	n.d.		
ovid-16	Yes	Yes	Yes	*phi-32* *ssl-1*	Pro75Ser Gly1119Glu	Ubiquitin gene SNF2-related

n.s., not scored. n.d., not determined.

FIGURES

Figure 1 | A forward genetic screen identifies novel antiviral immunity genes

a, Diagram of the *lys-3p::gfp* viral stress sensor.

b, Ovid screen workflow. Transgenic animals carrying the viral stress sensor were mutagenized using EMS and F2 progeny were assayed. OrV, Orsay virus. Ovid, Orsay virus immunodeficient.

c, Top panel: viral load of strains as indicated, measured by qRT-PCR of OrV RNA1, 4 dpi. Bars represent average value; error bars represent the standard error of the mean (SEM) of four independent infections. One-tailed student's t-test: ****p<0.0001, *** p<0.001, **p<0.01, *p<0.05. Bottom panel: locomotion defects scored (paralyzed or twitching) after *unc-22* RNAi feeding. Bars: average value; error: SEM; three independent RNAi treatments. Two-tailed student's t-test: ****p<0.0001, **p<0.01.

d, Viral load compared to *sdz-6* mRNA levels by qRT-PCR. Dots: average value; error: SEM; four independent infections. Samples as in **c**.

Figure 2 | The terminal uridylyltransferase CDE-1 restricts viral infection

a, Diagram of *cde-1* alleles. DAD, catalytic dead mutant.

b, Neighbor joining tree of the terminal uridylyl transferases (TUTs) of *C. elegans* and humans and *S. pombe* CID1.

c, Diagrams of *C. elegans* CDE-1 and human TUT4 and TUT7. Domains were predicted by Interpro. The central D of the conserved DDD catalytic triad is highlighted in red.

d, Viral load as measured by qRT-PCR of OrV RNA1 genome in adults two days after infection. Boxplots: whiskers from minimum to maximum; dots: independent infection; n=5. One-tailed student's t-test: **** p<0.0001, **p<0.01

Figure 3 | CDE-1 acts in parallel to antiviral RNAi

a, Schematic of antiviral RNAi in *C. elegans*. Viral Recognition Complex (ViRC) includes DCR-1; DRH-1; RDE-4.

b, Comparison between the viral load and primary viRNA populations. Primary viRNAs (23-nucleotide long, from 5′ monophosphate RNA sequencing). Only antisense RNAs were considered to exclude potential viral genome degradation products. Dots: independent infection.

c, Comparison between the viral load and secondary viRNA populations. Secondary viRNAs (22-nucleotide long, starting with a G, from 5′ tri/monophosphate RNA sequencing). Samples as in **b**.

d and e, Viral load as measured by qRT-PCR of OrV RNA1 genome in adults two days after infection. Boxplots: whiskers from minimum to maximum; dots: independent infection; n=5. One-tailed student's t-test: *** $p<0.001$, ** $p<0.01$, * $p<0.05$. Samples as in **b**.

Figure 4 | CDE-1 directly targets the Orsay virus RNA genome for uridylation

a, Schematic of TUT-mediated RNA degradation.

b, Poly(A) tail length distribution measured by TAIL-seq after two days of OrV infection. Vertical bars: range from minimum to maximum (two independent *C. elegans* culture plates). Vertical grey line represents the mean of *cde-1* and wild type peaks (38 nt).

c, Schematic of Orsay virus replication

d, Most frequent collapsed reads after RACE-seq on OrV RNA1 and RNA2 (2 dpi), respectively. Non-templated residues (absent from the reference genome) are indicated in red.

e, Percentage reads with non-templated nucleotides detected at the 3′ end of OrV RNA1-2 in strains as indicated, two days post infection. Two independent infections per genotype.

f, Percentage reads with a non-templated mono-uridyl residue at the 3′ end of OrV RNA2, upon RNAi-mediated gene knockdown as indicated, one day post infection. Bars; average; dots: independent RNAi treatments and infections.

Figure 5 | Antiviral RNAi and virus terminal uridylation are parallel immune defense pathways in *C. elegans*. Virion cartoon adapted from [12]. The Orsay virus primarily infects intestinal cells in *C.* elegans[9]. Once entered in the host cell, the virus disassembles in the cytoplasm and exposes its RNA genome. The Orsay virus has a bipartite positive-stand RNA genome that can be directly translated by the cellular machinery. The Orsay RNA1 molecule encodes a viral RNA dependent RNA polymerase (RdRP) and the Orsay RNA2 molecule encodes the capsid protein[4]. Virus amplification occurs in the cytoplasm in two steps: (i) the positive-strand genome serves as a template for the synthesis of a negative strand antigenome by the viral RdRP; (ii) the antigenome serves, in turn, as a template for further synthesis of genomic RNAs. The *C. elegans* antiviral RNAi response is initiated by DCR-1–DRH-1–RDE-4 (Viral RNA Recognition Complex) that recognize replicating double-stranded viral RNAs and process them into virus-derived small interfering RNAs (primary viRNAs). Primary viRNAs are loaded into the RDE-1 Argonaute protein and trigger the synthesis of secondary viRNAs by the host RdRP RRF-1, that uses the viral RNA as a template. Secondary viRNAs, loaded into somatic Argonaute proteins (SAGOs), target viral RNAs by base complementarity and potently reduce virus replication[5,11]. Viral RNAs are also targeted by the terminal uridylyltransferase CDE-1. CDE-1 marks viral RNAs with a 3′ U-tail to recruit 5′ to 3′ exonucleases of the XRN family, and 3′ to 5′ exonucleases of the exosome complex. *C. elegans* may have additional antiviral pathways, for example a set of stress response genes is induced by a STAT signaling pathway upon virus infection, that could promote virus clearance (not shown in this model) [15,16].

Figure 6 | The terminal uridylyltransferases TUT4(7) attenuate Influenza A mRNAs in mammalian cells

a, Schematic of Influenza A virus replication

b-d, Most frequent collapsed reads after RACE-seq on IAV NP cRNA, NP vRNA and NP mRNA, respectively in A549 cells at 8 hpi.

e, Percentage of reads with a non-templated U-tail (no U-tail; 1 U; 2 Us or ≥ 3 Us) in different RNAs as indicated measured by RACE-seq in A549 cells 8 hpi.

f, Percentage of reads with a non-templated U-tail (as in **e**) in MEF cells of different genotypes as indicated (with two independently created cell lines per genotype).

g-h, Percentage of infected cells measured by immunofluorescence against NP (FACS). Bars: average; Error: SEM; three independent infections. MEFs *Tut4(7)* KO are full null independent lines.

Figure 1. Le Pen et al.

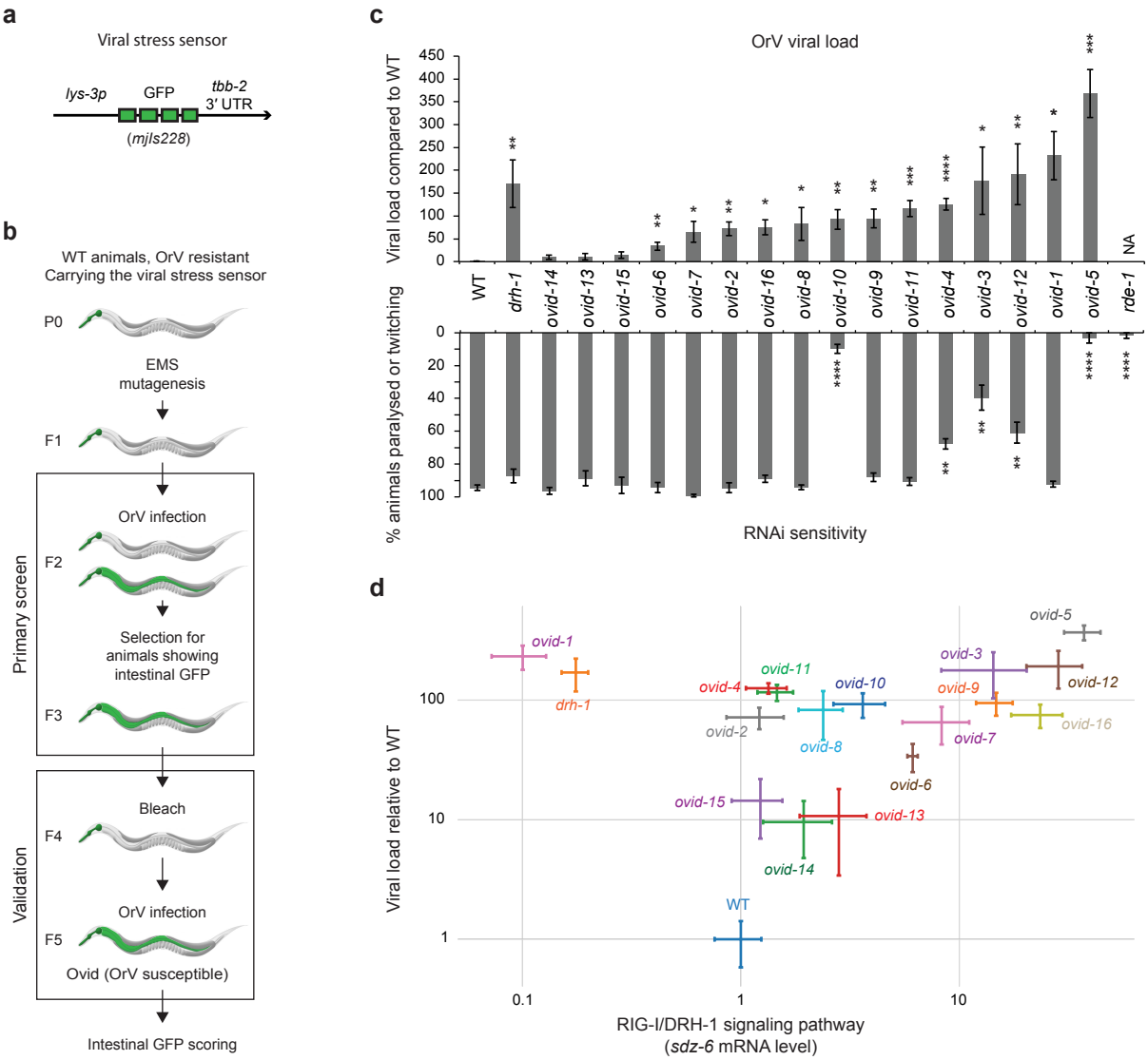

Figure 2. Le Pen et al.

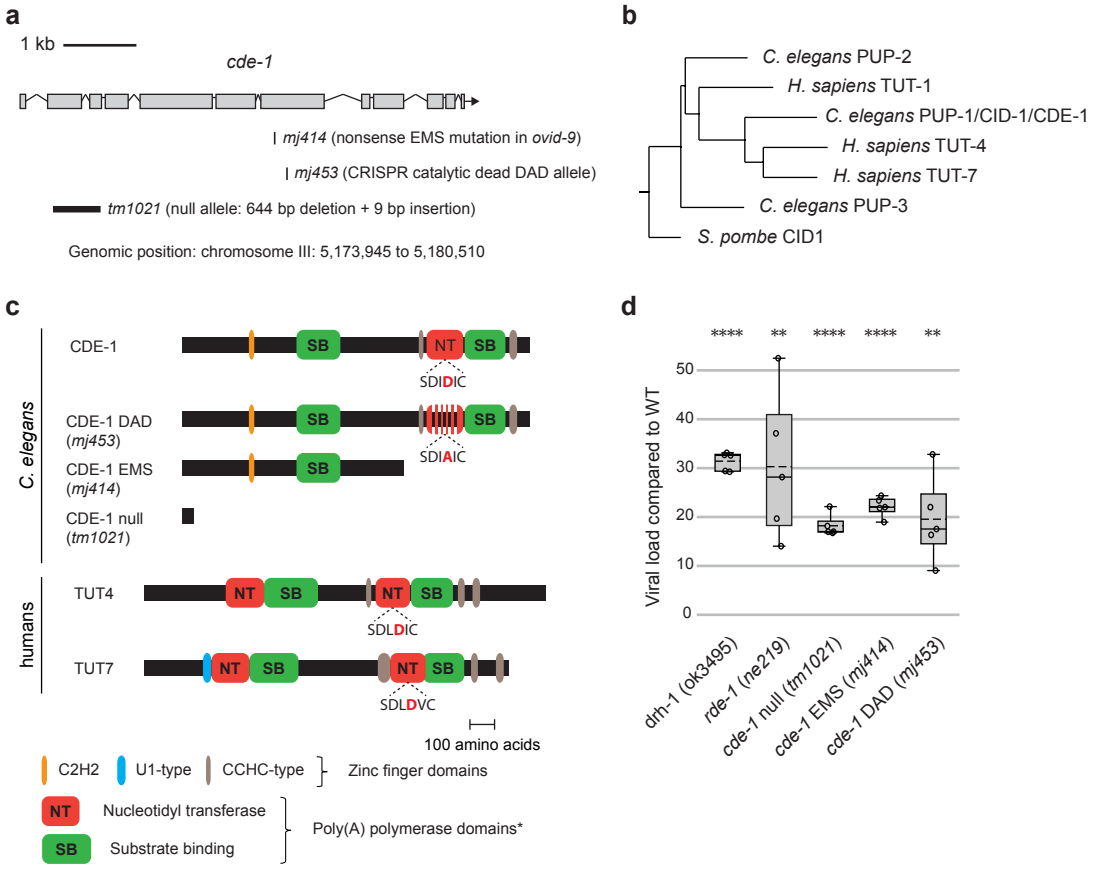

Figure 3. Le Pen et al.

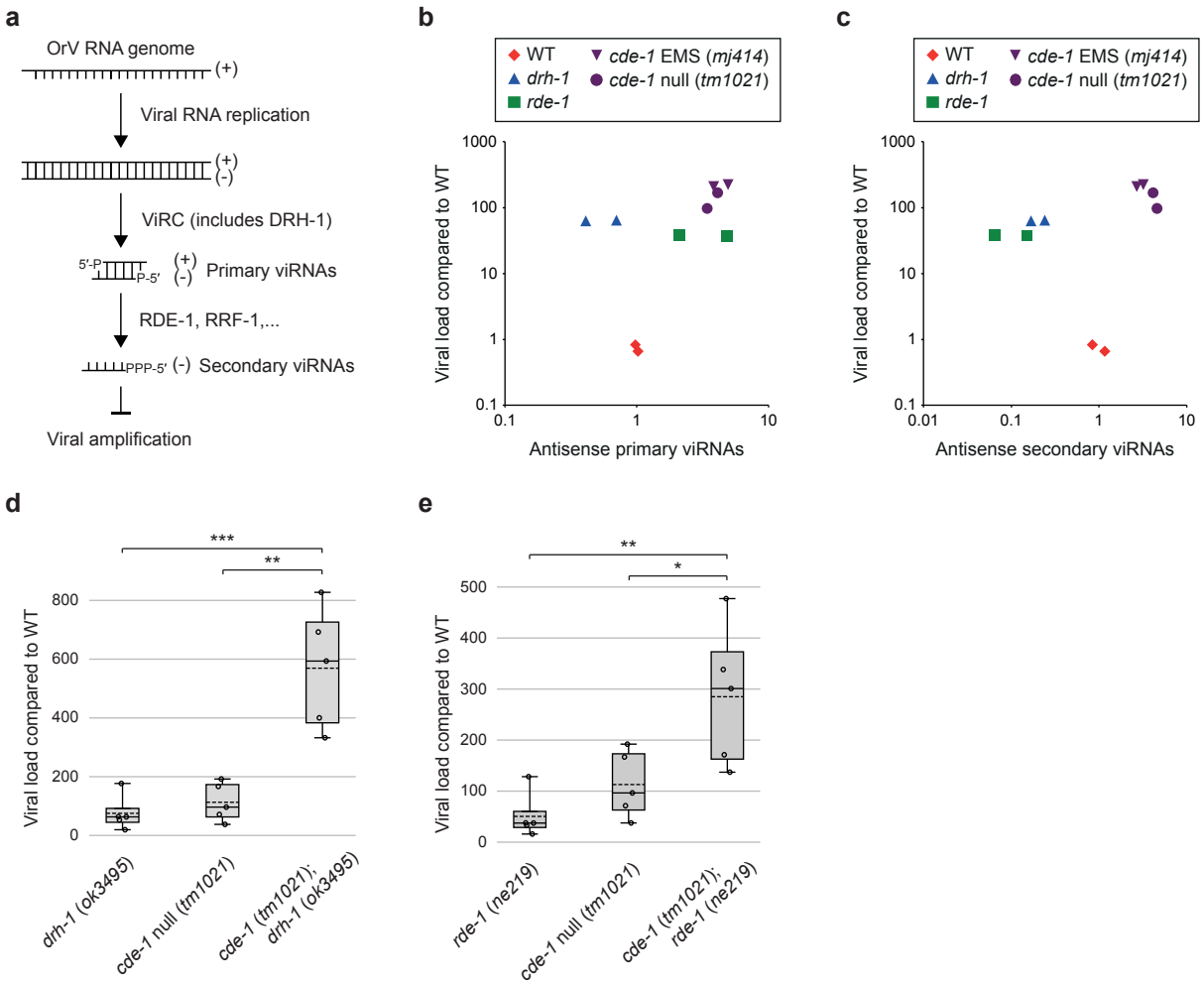

Figure 4. Le Pen et al.

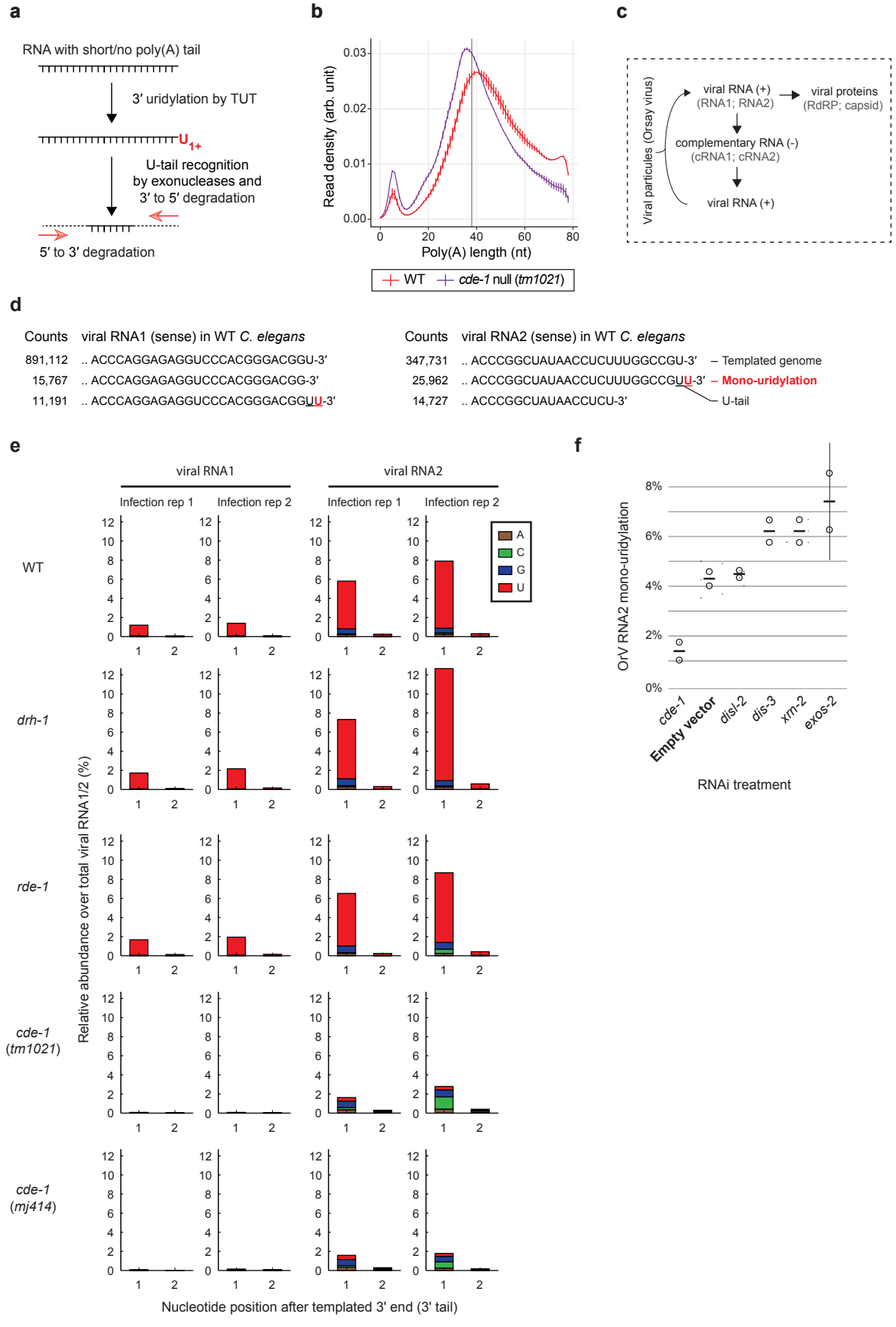

Figure 5. Le Pen et al.

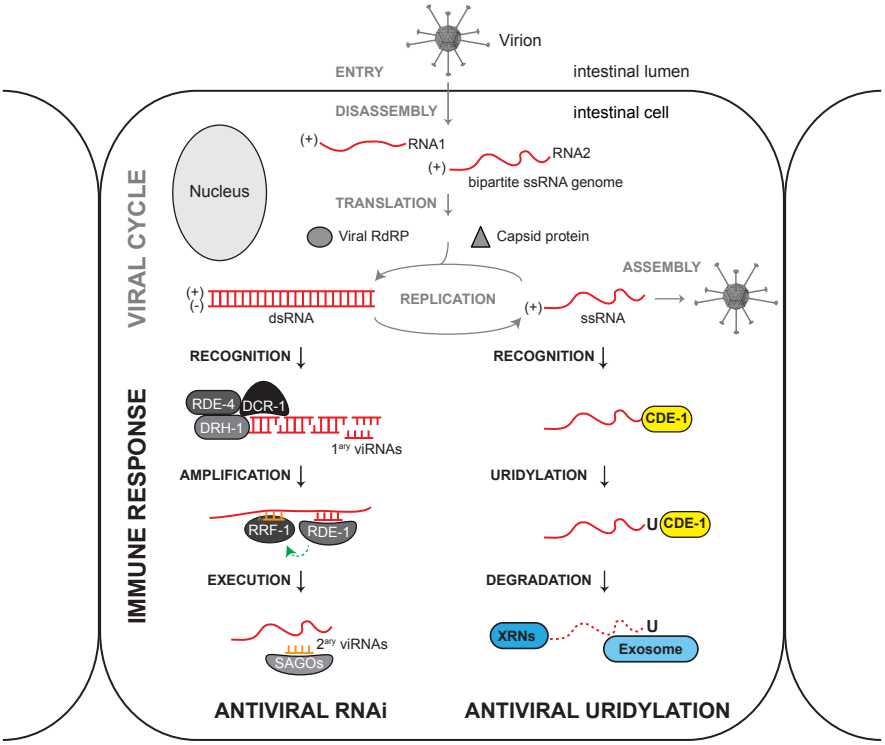

Figure 6. Le Pen et al.

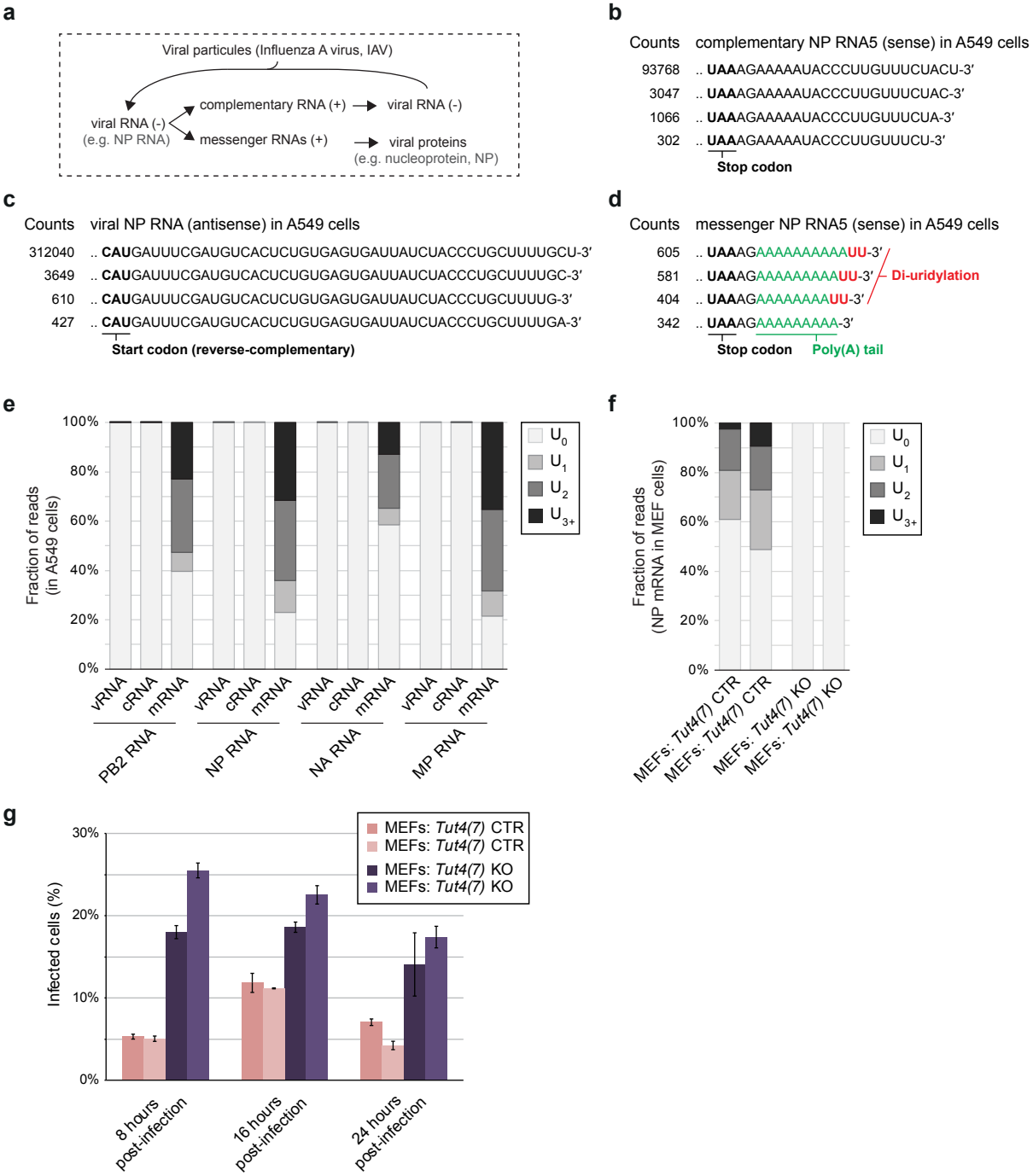

INTEGRATED SUPPLEMENTARY FIGURE TEMPLATE

Supplementary figures and legends are not edited or styled by the journal, so please follow the same style guidelines provided for figures in the main text. If there are five or more main-text figures, the number of supplementary figures should not exceed the number of main-text figures. If there are four or fewer main-text figures, up to five supplementary figures are allowed.
Please Submit this form as a word document

Titles for Supplementary Figures should be a single sentence and should not contain panel descriptions, reference citations or abbreviations that are not defined in the main text.

Cite any associated references internally in the legend text, e.g., “as shown previously (Author, A. *et al.*, *Journal.* **11**, 1–12, 2015).”

Click inside this box and **insert a single image for Supplementary Figure 1**.

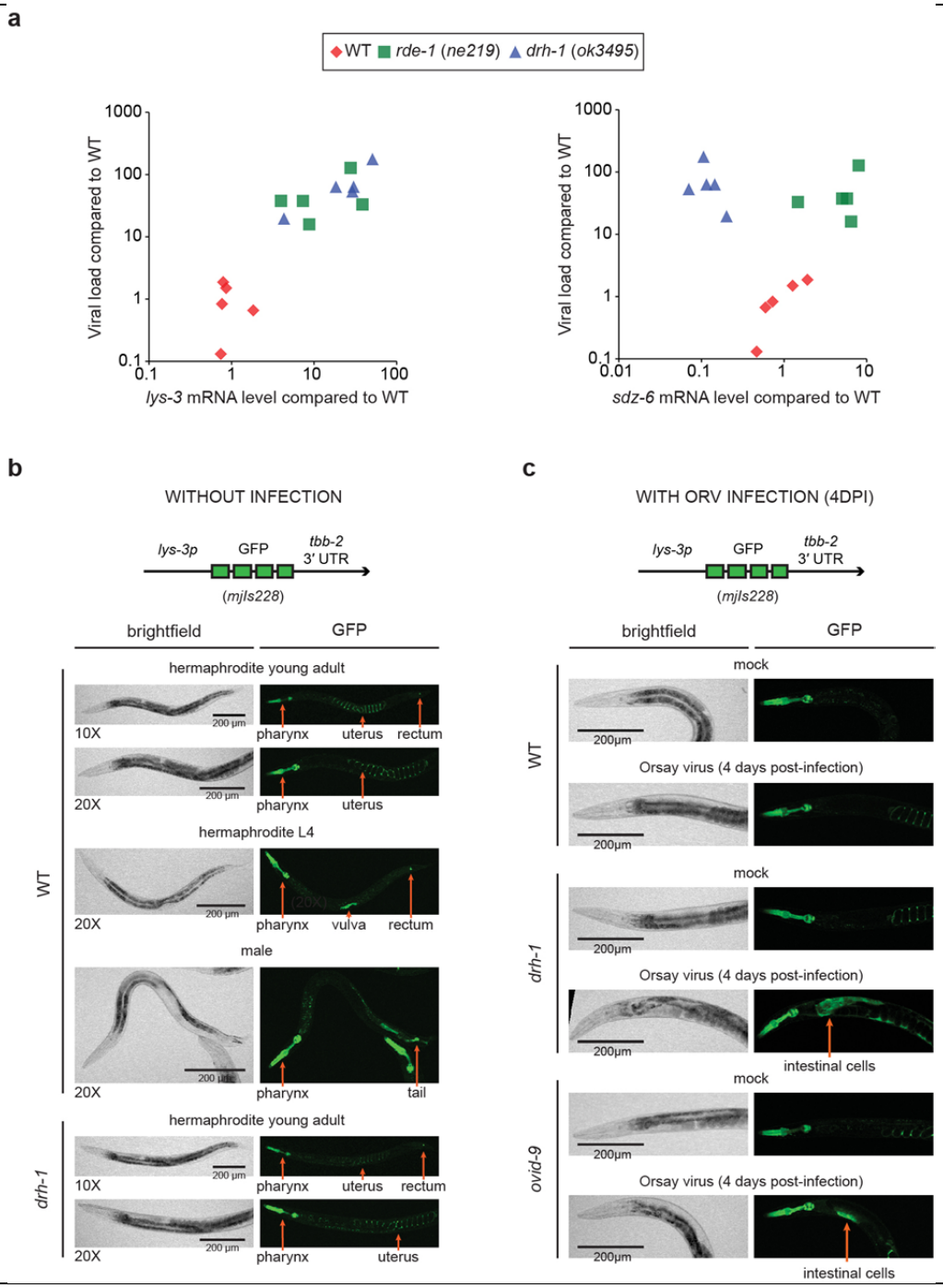

Supplementary Figure 1

The viral stress sensor (*lys-3p::GFP*) is constitutively active in some tissues but is induced in the intestine upon severe viral infection.

a, Comparison of viral load and the *lys-3* and *sdz-6* mRNA expression after two days of infection by qRT-PCR, strains as indicated. Dots: independent infection. Samples as in Fig. 3d,e.

b, Representative confocal sections (10× or 20× magnification, as specified) of the viral stress sensor in wild type and *drh-1* mutants without infection. The viral stress sensor exhibited constitutive activity in uninfected individuals, which was restricted to specific tissues. GFP was observed at all developmental stages in the pharynx and the rectum of hermaphrodites. Additionally, hermaphrodites at the L4 larval stage would show a strong GFP signal around the vulva and gravid adults exhibited the GFP in the uterine lumen. In males, GFP was observed in the pharynx and the tail. GFP expression was comparable in wild type and *drh-1* mutants and independent of viral infection. Thus, the gene *lys-3* is constitutively active in tissues neighboring openings exposed to the environment, the most likely entry points of potential bacterial pathogens.

c, Representative confocal sections (20× magnification) of young adults (strains as indicated) carrying the viral stress sensor. Animals were uninfected (mock) or infected with OrV for four days. The viral stress sensor was strongly induced in the intestine after infection of *drh-1* mutants, which is in agreement with the tropism of OrV. Intestinal GFP was most often visible around the collar of the nematodes, in the anterior region of the intestine in young adults. Some infected individuals exhibited a strong GFP signal throughout their entire body (data not shown), suggesting that the induction of the viral stress sensor can spread from cell to cell, like an inflammation process. The viral stress sensor offers an opportunity to easily monitor viral infections in living animals.

Click inside this box and **insert a <u>single image</u> for Supplementary Figure 2**.

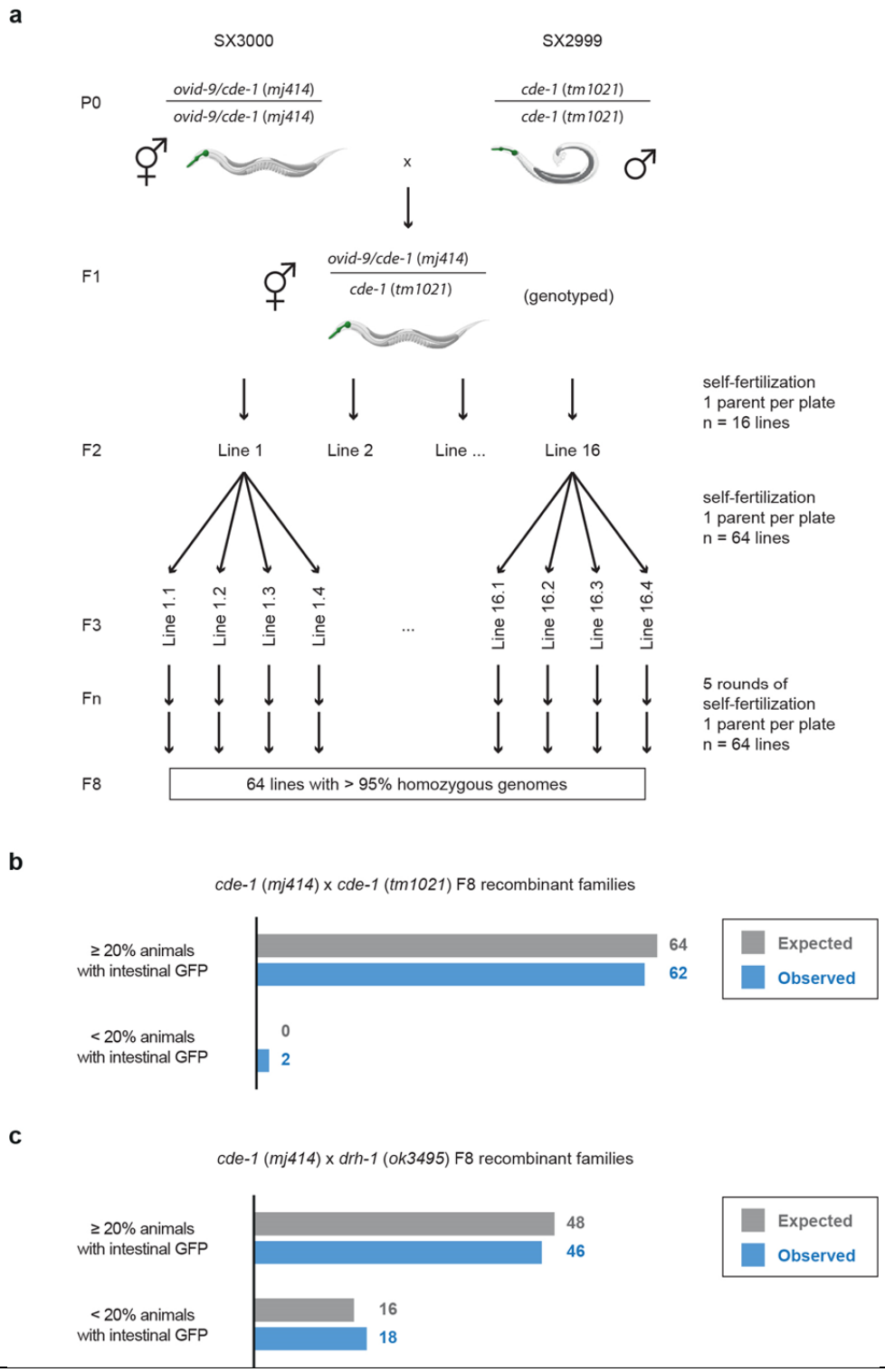

Supplementary Figure 2

A *cde-1* deletion allele fails to complement the screen isolate *ovid-9*.

a, Workflow of *cde-1*/*ovid-9* (*mj414*) × *cde-1* (*tm1021*) F8 recombinant family generation. A similar strategy was used to construct the *cde-1* (*mj414*) × *drh-1* (*ok3495*) F8 recombinant families. All animals were homozygous for the viral stress sensor (*mjIs228*).

b-c, Number of families that activated the viral stress sensor in more than 20% of individuals after four days of infection with OrV. Approximately 50 individuals scored per family. Bars: number of families meeting criteria as indicated.

Click inside this box and **insert a <u>single image</u> for Supplementary Figure 3**.

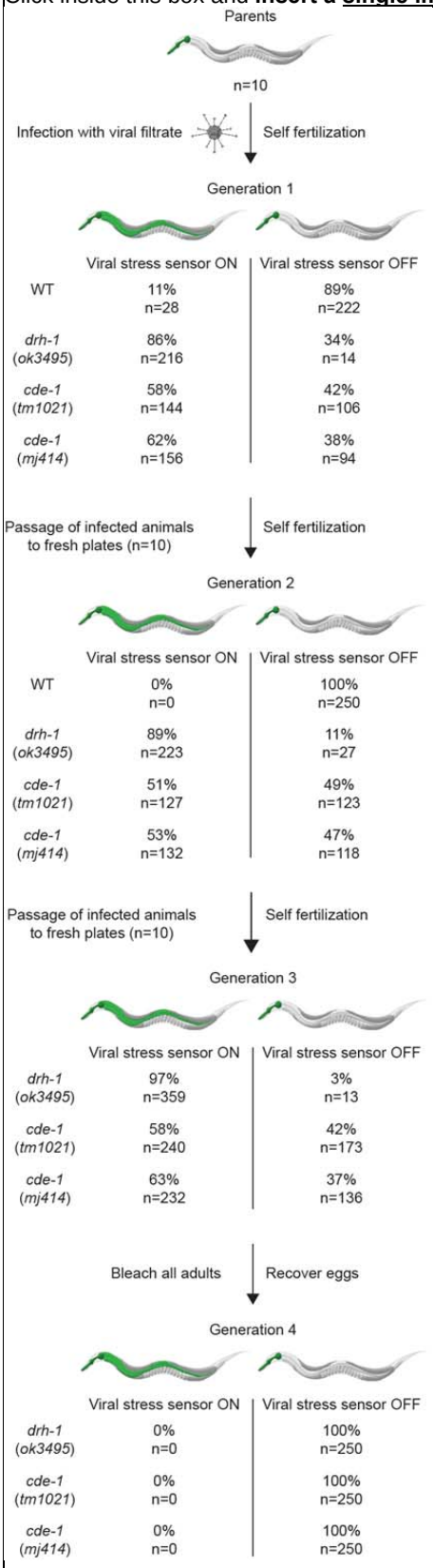

Supplementary Figure 3

***cde-1* mutants show horizontal transmission of Orsay virus infection.**

Workflow and data monitoring the inter-individual transmission of OrV infection (in strains as indicated) using the viral stress sensor.

Click inside this box and **insert a single image for Supplementary Figure 4**.

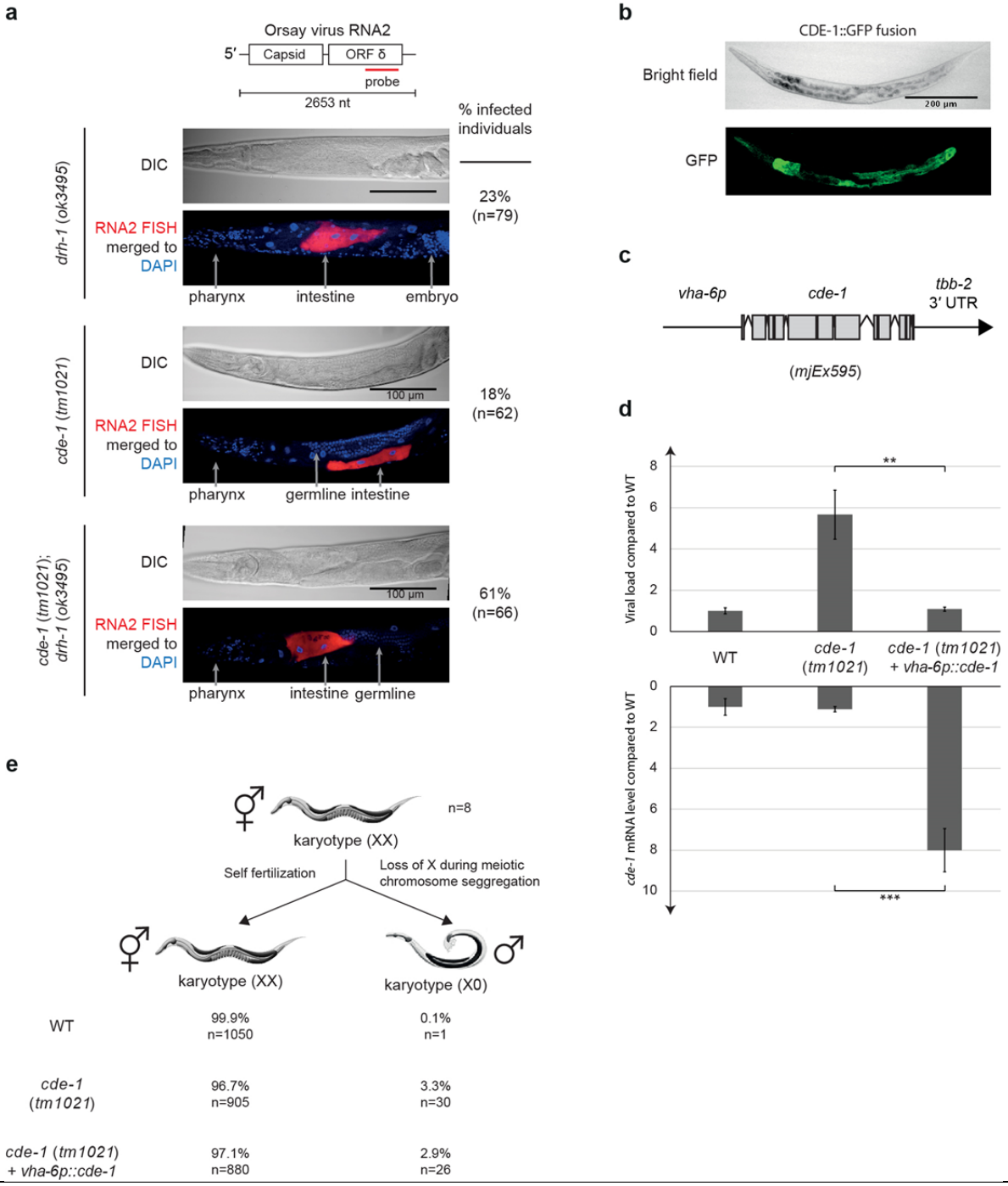

Supplementary Figure 4

Intestinal expression of *cde-1* confers antiviral immunity.

a, Representative confocal sections (20× magnification) of OrV *in vivo* RNA FISH.

b, Representative confocal section (10× magnification) of a C. elegans L4 larva expressing cde-1::GFP. As two previous reports disagreed about the expression pattern of CDE-1 (Olsen, A. *et al*. *Science* 312, 1381–1385, 2006; van Wolfswinkel, J. C. *et al*. *Cell* 139, 135–148, 2009), we used fosmid-recombineering to generate transgenic animals driving GFP expression from an endogenous genomic context.

c, Diagram of the *cde-1* rescue transgene, using the intestine-specific promoter of the gene *vha-6*. This transgene was injected in *cde-1* null mutants.

d, Viral load as measured by qRT-PCR of OrV RNA1 genome in adults two days after infection. Bars: average value; error: SEM; five independent infections. One-tailed student's t-test: *** $p<0.001$, ** $p<0.01$.

e, Incidence of male in the progeny of hermaphrodites left to self-fertilize at 25°C, in strains as indicated.

Click inside this box and **insert a single image for Supplementary Figure 5**.

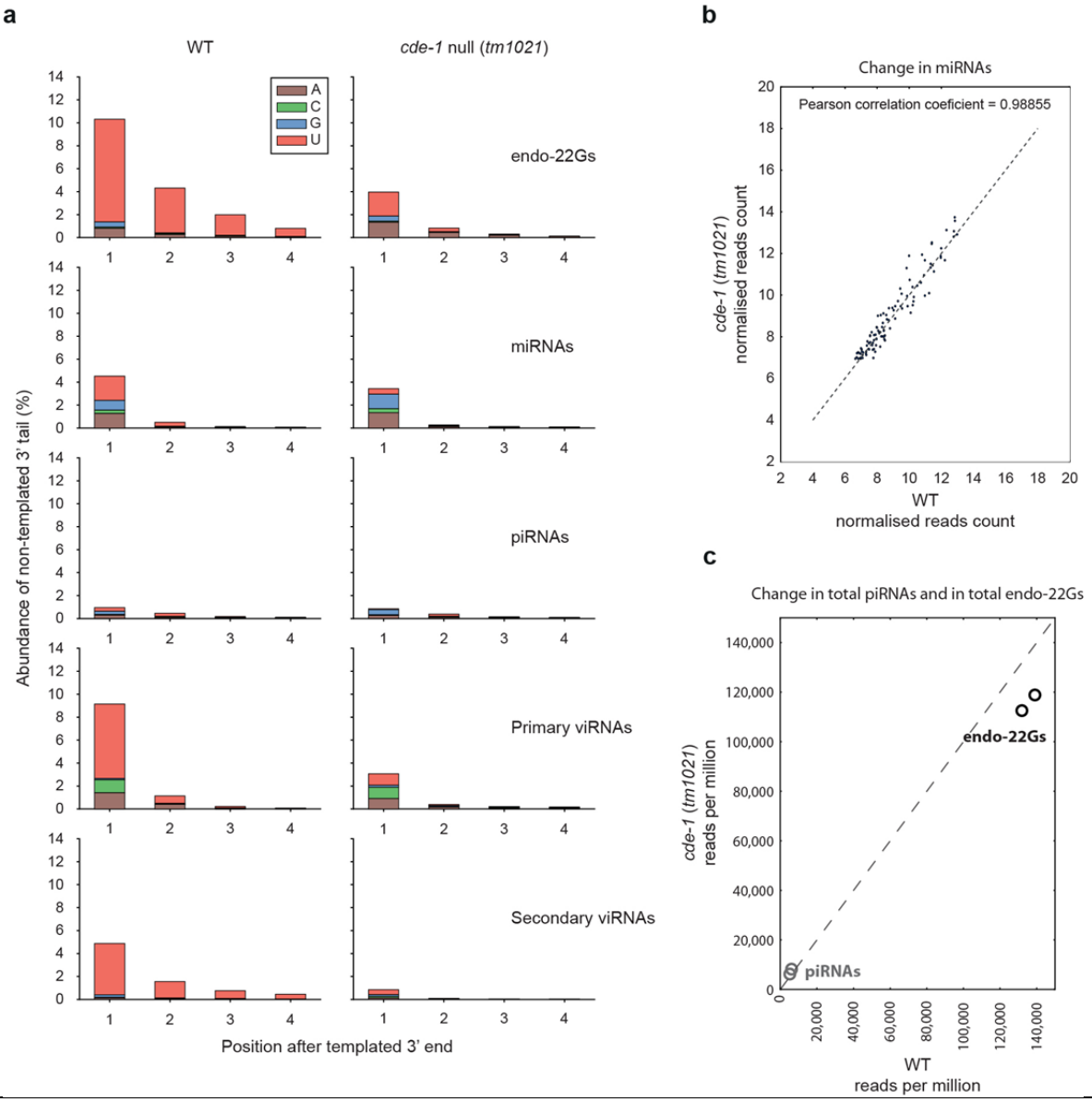

Supplementary Figure 5

CDE-1 is not required for general miRNA homeostasis.

a, Non-templated nucleotides at the 3' end of the different classes of endogenous and antiviral small RNAs as indicated. RNA was isolated from young adults after two days of infection with OrV.

b, miRNA expression in *cde-1* (*tm1021*) mutants as compared to wild type, samples as in **a**. Dots: individual miRNA; reads per million averaging two independent *C. elegans* culture plates.

c, piRNAs and endogenous 22G-RNAs abundance in *cde-1* (*tm1021*) mutants as compared to wild type, normalised to library size. Dots: independent *C. elegans* culture plate. Samples as in **a**.

Click inside this box and **insert a single image for Supplementary Figure 6**.

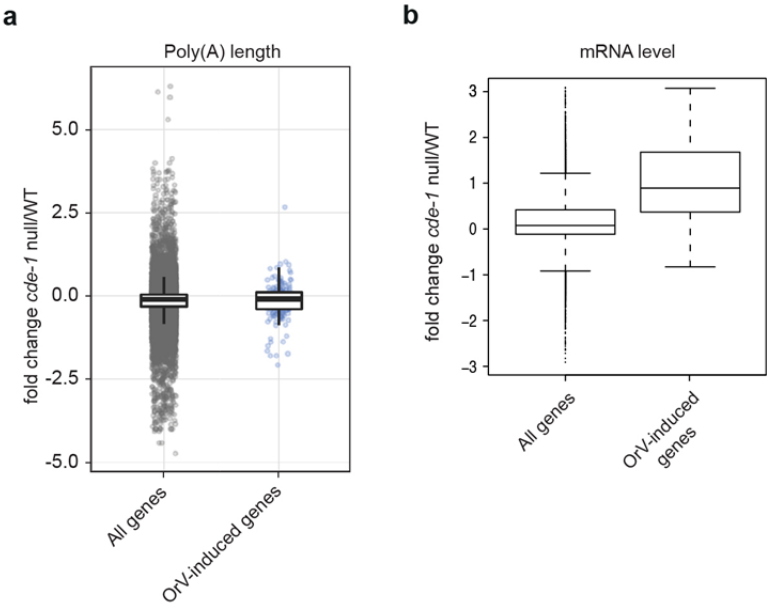

Supplementary Figure 6

CDE-1-depleted animals show a high expression of stress response genes during Orsay virus infection

a, Fold change in the length of poly(A) tails (measured by TAIL-seq) in *cde-1* mutants compared to wild type. RNA was isolated from young adults after two days of OrV infection. Turkey boxplot.

b, Differential mRNA expression in *cde-1* (*tm1021*) compared to wild type, two days of OrV infection (mRNA-seq). Turkey boxplot; dots: outliers.

Click inside this box and **insert a single image for Supplementary Figure 7**.

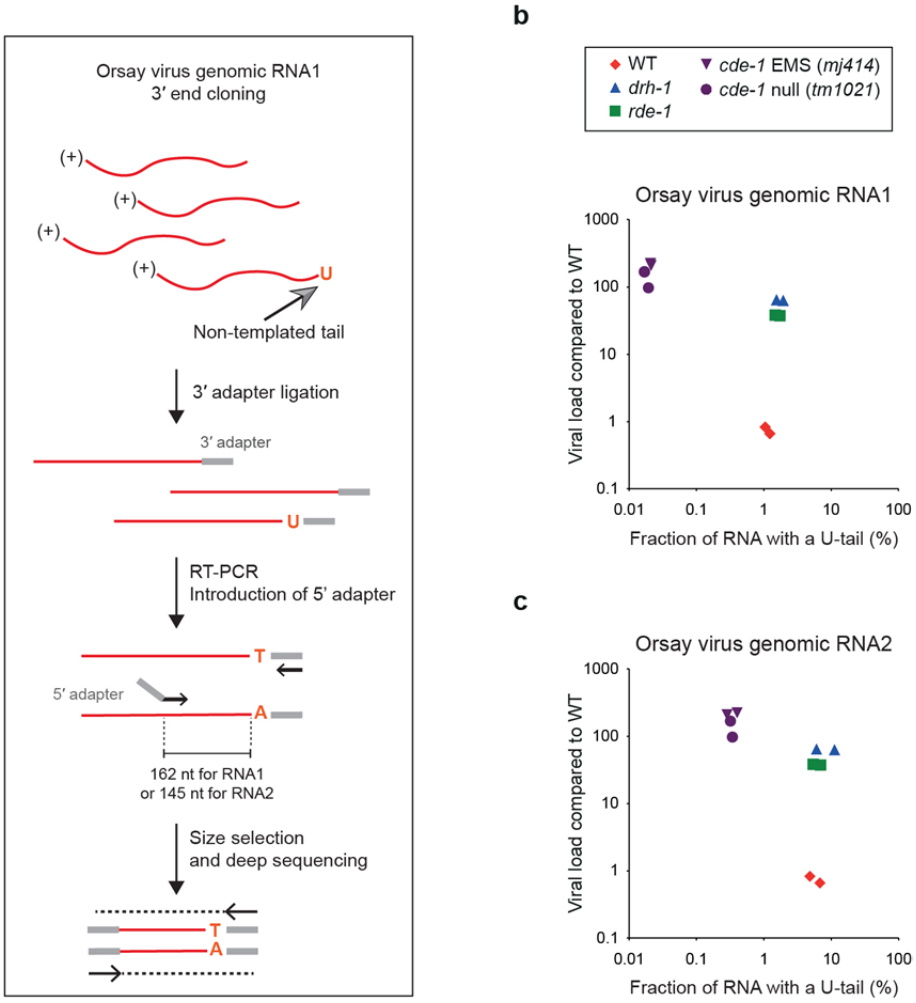

Supplementary Figure 7

The 3' end of the Orsay virus genome contains CDE-1-dependent non-templated U-tails

a, Simplified workflow of 3' RACE-seq of OrV RNA1 and OrV RNA2.

b-c, Comparison between the viral load and the fraction of non-templated mono(U) tails at the 3' end of OrV RNA1 and OrV RNA2, respectively, in strains as indicated. Dots: independent infection. Samples as in Fig. 3d,e and Fig. 4e.

Click inside this box and **insert a single image for Supplementary Figure 8**.

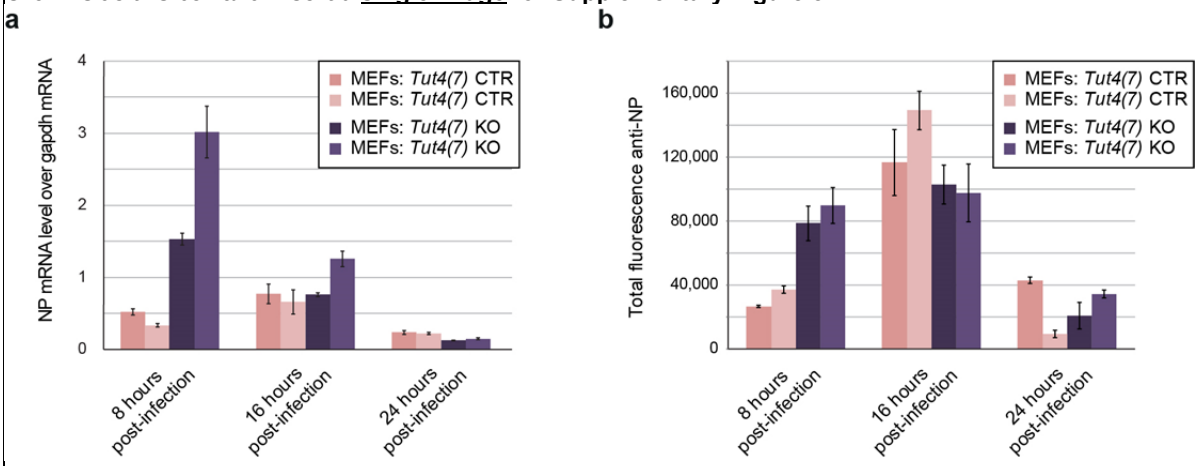

Supplementary Figure 8

The terminal uridylyltransferases TUT4(7) restrict Influenza A infection

a, Protein level of the IAV NP measured by immunofluorescence (FACS). Error: SEM in three independent infections.

b, Level of expression of the IAV NP mRNA normalized to *Gapdh* in MEF cells of different genotypes as indicated. Bars: average value; error: SEM; three independent infections.

1

Supplementary Table 1 | Infection by the Orsay virus induces viral stress sensor in Ovid screen isolates.

Strain	Genotype	% intestinal GFP mock	% intestinal GFP OrV
SX2635	WT	0	4
SX2615	*rde-1*	0	42
SX2790	*drh-1*	0	83
SX2996	*ovid-1*	0	86
SX2900	*ovid-2*	0	83
SX2739	*ovid-3*	0	74
SX2901	*ovid-4*	0	73
SX2902	*ovid-5*	0	68
SX2729	*ovid-6*	0	64
SX2991	*ovid-7*	0	60
SX2990	*ovid-8*	0	52
SX3000	*ovid-9*	0	48
SX2881	*ovid-10*	0	47
SX2987	*ovid-11*	0	46
SX2988	*ovid-12*	0	44
SX2920	*ovid-13*	0	26
SX2909	*ovid-14*	0	26
SX2886	*ovid-15*	0	24
SX2885	*ovid-16*	0	24

The percentage of young adults exhibiting intestinal GFP was assessed after four days of infection by OrV or in non-infected animals (mock). 20 to 50 young adults were scored per plate, in three independent infections (average values are shown here). The screen isolates *ovid-1,7,8,9,11,12* were backcrossed prior to GFP scoring (see Supplementary Table 2).

Supplementary Table 2 | *C. elegans* strains used in this study

Genotype	Strain	Comment
+	N2	
cde-1(*mj453*) III	SX3186	
cde-1(*tm1021*) III	RF1290	
cde-1(*tm1021*) III ; *drh-1*(*ok3495*) IV	SX2998	
cde-1(*tm1021*) III ; mjEx595	SX3265	Contains the intestine-specific *cde-1* construct (*vha-6p::cde-1*)
cde-1(*tm1021*) III ; *mjIs228* ?	SX2999	
cde-1(*tm1021*) III ; *rde-1*(*ne219*) V	SX3004	
drh-1(*ok3495*) IV	RB2519	
drh-1(*ok3495*) IV ; *mjIs228* ?	SX2790	
F27D4.6(*tm1098*) I	FX01098	
mjEx594 ?	SX3123	Contains the *cde-1::GFP* fosmid (TransgeneOme construct)
mjIs228 ?	SX2635	Contains the biostress (*lys-3p::GFP*) reporter
ovid-1(*mj417*)	SX2996	Backcrossed 2X to SX2635
ovid-2(*mj422*)	SX2900	
ovid-3(*mj367*)	SX2739	
ovid-4(*mj423*)	SX2901	
ovid-5(*mj425*)	SX2902	
ovid-6(*mj357*)	SX2729	
ovid-7(*mj405*)	SX2991	Backcrossed 2X to SX2635
ovid-8(*mj369*)	SX2990	Backcrossed 2X to SX2635
ovid-9(*mj414*)	SX3000	Backcrossed 2X to SX2635
ovid-10(*mj403*)	SX2881	
ovid-11(*mj354*)	SX2987	Backcrossed 3X to SX2635
ovid-12(*mj401*)	SX2988	Backcrossed 3X to SX2635
ovid-13(*mj432*)	SX2920	
ovid-14(*mj431*)	SX2909	
ovid-15(*mj408*)	SX2886	
ovid-16(*mj407*)	SX2885	
rde-1(*ne219*) V	WM27	
rde-1(ne219) V ; *mjIs228 ?*	SX2615	

Supplementary Table 3 | Primers used in this study

Name	Sequence	Description
M1835	TGGAGCCGACTATGTCGTTGAG	RT-qPCR on *gapdh* - left
M1836	GCAGATGGAGCAGAGATGATGAC	RT-qPCR on *gapdh* - right
M4410	ACCTCACAACTGCCATCTACA	RT-qPCR OrV RNA1 - left
M4411	GACGCTTCCAAGATTGGTATT	RT-qPCR OrV RNA1 - right
M4988	CAATGCATTTGAAGCTGGAC	RT-qPCR on *lys-3* - left
M4989	CCATTAGCAAGCAAATTCTGG	RT-qPCR on *lys-3* - right
M5041	ACAATCGGGCGTTCAATTC	RT-qPCR on *sdz-6* - left
M5042	TCTGATAGCTGGCTGAGTGG	RT-qPCR on *sdz-6* - right
M5472	GGGGACAACTTTGTATAGAAAAGTT GCTTCGAAAGAAACCCAATCCTC	cloning of *lys-3p* into gateway system - left
M5473	GGGGACTGCTTTTTTGTACAAACTT GGAGGAGCTGGGAAAGAGTAGCA	cloning of *lys-3p* into gateway system - right
M7316	CCGGAACCCATCACGAAATT	PCR on *cde-1* (*mj414*) for Sanger sequencing - left
M7317	TCCATTTCAAAGTCTCCACAGA	PCR on *cde-1* (*mj414*) for Sanger sequencing - right
M7454	ATGGCCAAACGTCTGAAACC	OrV RNA1 3' RACE - left
M7455	CCAAAGTCGCTTGCTGTACA	OrV RNA2 3' RACE - left
M7456	CCTTGGCACCCGAGAATTCCA	OrV RNA1/2 3' RACE - right
M7601	GTTCAGAGTTCTACAGTCCGACGAT CATGGCCAAACGTCTGAAACC	OrV RNA1 3' RACE (with TruSeq RA5 sequence) - left
M7602	GTTCAGAGTTCTACAGTCCGACGAT CCCAAAGTCGCTTGCTGTACA	OrV RNA2 3' RACE (with TruSeq RA5 sequence) - left
M8443	GCTAATTGGGCAAGGAGACG	IAV 3' RACE PB2 RNA complementary left
M8444	GCTGGGTTCTTCTCCTGTCT	IAV 3' RACE PB2 RNA genomic left
M8451	CTCTCGGACGAAAAGGCAAC	IAV 3' RACE NP RNA complementary left
M8452	AAGTTCGGTGCACATTTGGA	IAV 3' RACE NP RNA genomic left
M8453	CGCAATCTGGACTAGTGGGA	IAV 3' RACE NA RNA complementary left
M8454	GCCTTGGTTGCATATTCCAGT	IAV 3' RACE NA RNA genomic left
M8455	ACGGTTTGAAAAGAGGGCCT	IAV 3' RACE MP RNA complementary left
M8456	CGGTGTTCTTCCCTGCAAAG	IAV 3' RACE MP RNA genomic left
M8459	GTTCAGAGTTCTACAGTCCGACGAT Cgctaattgggcaaggagacg	IAV 3' RACE PB2 RNA complementary left (with TruSeq RA5 sequence)

M8460	GTTCAGAGTTCTACAGTCCGACGAT Cgctgggttcttctcctgtct	IAV 3' RACE PB2 RNA genomic left (with TruSeq RA5 sequence)
M8467	GTTCAGAGTTCTACAGTCCGACGAT Cctctcggacgaaaaggcaac	IAV 3' RACE NP RNA complementary left (with TruSeq RA5 sequence)
M8468	GTTCAGAGTTCTACAGTCCGACGAT Caagttcggtgcacatttgga	IAV 3' RACE NP RNA genomic left (with TruSeq RA5 sequence)
M8469	GTTCAGAGTTCTACAGTCCGACGAT Ccgcaatctggactagtggga	IAV 3' RACE NA RNA complementary left (with TruSeq RA5 sequence)
M8470	GTTCAGAGTTCTACAGTCCGACGAT Cgccttggttgcatattccagt	IAV 3' RACE NA RNA genomic left (with TruSeq RA5 sequence)
M8471	GTTCAGAGTTCTACAGTCCGACGAT Cacggtttgaaaagagggcct	IAV 3' RACE MP RNA complementary left (with TruSeq RA5 sequence)
M8472	GTTCAGAGTTCTACAGTCCGACGAT Ccggtgttcttccctgcaaag	IAV 3' RACE MP RNA genomic left (with TruSeq RA5 sequence)
M8652	CCTTCCACAATGCCAAAGTT	gapdh gene specific RT primer
M8581	CCAGATCGTTCGAGTCGTTTTTTTT TTTTTTTTTCTTTAATTGTC	IAV NP mRNA gene specific RT primer
M8651	GGGTGTGAACCACGAGAAAT	gapdh qRT-PCR primer left
M8652	CCTTCCACAATGCCAAAGTT	gapdh qRT-PCR primer right
M8582	CCAGATCGTTCGAGTCGT	IAV NP mRNA qRT-PCR primer left
M8583	CGATCGTGCCCTCCTTTGCGATCGT GCCCTCCTTTG	IAV NP mRNA qRT-PCR primer right
HJ359	GATGGACAAACAGACAAACC	Tut4-1GTF genotyping
HJ360	GCAGTTGTGCTATATTGACTC	Tut4-1GTR genotyping
HJ365	TGATCAGAGCATGCATACTC	Tut7-2GTF genotyping
HJ366	AAACAAGAAGCAGAGGTCCA	Tut7-2GTR genotyping